Republic of Iraq
Ministry of Higher Education
& scientific research
University of Babylon
College of Education for Pure Sciences
Department of Physics

The Effect of the Proton and Neutron as Probe for the Nuclear Fusion Reactions at Near-Barrier Energies

A Thesis
Submitted to the Council of College of Education for Pure Sciences, University of Babylon in Partial Fulfillment of the Requirements for the Degree of Master in Education/Physics

By

Muntazer Ahmed Khaudhier Hasan

(B.Sc. in Physics, University of Babylon, 2020)

Supervised By

Prof.Dr. Fouad A. Majeed

2023 A.D. **1445 A.H.**

بِسْمِ اللَّهِ الرَّحْمَنِ الرَّحِيمِ

فَتَعَالَى اللَّهُ الْمَلِكُ الْحَقُّ وَلَا تَعْجَلْ بِالْقُرْآنِ مِن قَبْلِ
أَن يُقْضَىٰ إِلَيْكَ وَحْيُهُ وَقُل رَّبِّ زِدْنِي عِلْمًا

صَدَقَ اللهُ العَلِيُّ العَظِيم

سورة طه / آية ١١٤

Supervisors Certificate

We certify that this thesis, entitled (**The Effect of the Proton and Neutron as Probe for the Nuclear Fusion Reactions at Near-Barrier Energies)** was prepared by the student (**Muntazer Ahmed Khaudhier Hasan)** under our supervision at the College of Education for pure sciences, University of Babylon in partial fulfillment of the requirements for the Degree of Master Education in Physics.

Signature:
Name: Dr. Fouad A. Majeed
Title: Professor
(Supervisor)
Date: / /2023

Head of the Department Certificate

In view of the available recommendation, I forward this thesis for debate by the examining committee.

Signature:
Name: Dr. Khalid H. Abbas
Title: Professor
(Head of Physics Department)
Date: / / 2023

Dedication

This thesis is a product of support and inspiration from those close to me.

I express my heartfelt gratitude to my beloved parents who were my pillars of strength.

I am grateful to Almighty Allah for endowing me with the guidance, strength, power of mind, and protection to complete this study while maintaining good health.

Muntazer

Acknowledgments

I am grateful to Allah, the Lord of all creation, for granting me the physical and mental capacity to undertake this thesis.

I extend my sincerest thanks to my supervisor, Prof. Dr. Fouad A. Majeed, for his unwavering commitment, guidance, and expertise in my research area, his suggestions and constructive criticism have greatly enhanced the quality of this thesis.

I am also indebted to the staff members of the Department of Physics at the College of Education for Pure Sciences, as well as the Dean of the College of Education for Pure Sciences, for their kind assistance and support.

Muntazer

Abstract

In the current work, calculations have been carried out for the cross-section, total fusion σ_{fus}, fusion barrier distribution D_{fus}, and fusion probability P_{fus} by using both the quantum mechanical and semi-classical approaches for the systems ^{28}Si+^{90}Zr, ^{28}Si+^{92}Zr, ^{28}Si+^{94}Zr, ^{28}Si+^{96}Zr, ^{32}S+^{90}Zr, ^{32}S+^{96}Zr, ^{35}Cl+^{92}Zr, ^{41}K+ ^{28}Si, ^{45}K+ ^{28}Si, ^{44}Ar+^{28}Si, ^{41}K+^{16}O that involving one neutron or one proton transfer reactions.

The quantum mechanical and semi-classical approaches involved the use of the Brillouin, Kramers, and Wenzel (WKB) approximation to describe the relative motion between the projectile and target nuclei, and the Continuum Discretized Coupled Channel (CDCC) method of Alder-Winther (AW) to describe the intrinsic motion of the nuclei. For the semi-classical approach, calculations were made by using the computer program SCF (Sequential Complete Fusion), while for the quantum mechanical approach, calculations were made by using the computer program CC (Coupled-Channels) , and both programs are written by the programing language (Fortran 90).

The same Wood Saxon parameters for Akyüz Winter potential have been set for both approaches, and the results for both approaches have been compared with the measured experimental data, when adding the effect of coupling between the elastic and break-up channel.

The semi-classical approach calculations well described all the measured systems above the Coulomb barrier and the results below and around the Coulomb barrier have been improved when the coupling has been considered, while for the quantum mechanical approach, the coupling enhance the calculations above the “Coulomb barrier” and below the “Coulomb barrier” is very far and could not describe the data in most of the studied systems.

Content

List of Figures

List of tables

List of symbols and abbreviations

σ_{fus}	Total fusion cross-section fusion
D_{fus}	Barrier distribution
P_{fus}	Fusion probability
WKB	Brillouin, Kramers, and Wenzel
CDCC	Continuum Discretized Coupled Channel
AW	Alder-Winther
DCF	Direct Complete Fusion
SCF	Sequential Complete Fusion
ICF	Incomplete Fusion
NCBU	Non-Capture Breakup
CC	Couple channel
PQNT	Positive Q-value neutron transfer
V_b	Coulomb barrier
JWKB	Jeffreys-Wentzel-Kramers-Brillouin
Ec.m	Center of mass energy
LO-WKB	Lowest order WKB approximation
$\boldsymbol{V_N^{(0)}}$	The nuclear potential in entrance channels
$\mathbf{F(E)}$	Total fusion reaction cross-section through

r	Relative motion coordinate
μ	Reduced mass
V_o	The depth of the potential
a_0	Represents the potential diffuseness
R_n	The nuclear potential's radius
IWBC	Incoming wave boundary condition
$\boldsymbol{\xi}$	the set of intrinsic coordinates of the projectile and target nuclei
$\vec{\boldsymbol{r}}$	The separation vector of the colliding nuclei.
$\boldsymbol{H_0}$	The intrinsic Hamiltonian
T	Kinetic energy operator
$\|\boldsymbol{\beta}\rangle$	The eigenstates of the intrinsic Hamiltonian
Q(r)	Plane wave
A(r)	The amplitude of the wave function
$\boldsymbol{\delta}$Q(r)	The rate increase of the plane wave
$\boldsymbol{\psi^{WKB}(r)}$	The approximation wave function for the lowest order
$\boldsymbol{\psi}\ (\vec{\boldsymbol{r}}, \boldsymbol{\xi})$	The total wave function
$\boldsymbol{U}$	The interaction potential between the nuclei
$\vec{\boldsymbol{J}}_{\boldsymbol{\beta}}$	The probability of current density in channel $\boldsymbol{\beta}$

Chapter One

General Introduction and Literature Review

1.1 Introduction

Understanding the dynamic processes involved in fusion reactions on extremely short timescales, approximately ~10^{-21}s or shorter, is a significant challenge in nuclear physics. These processes heavily rely on the interaction barrier formed by the combination of Coulomb force, nuclear force, and centrifugal force between the nuclei. Describing these processes is complex due to the intricate nature of the interaction when the projectile undergoes tunneling or overcomes the internuclear barrier. In the energy range well above the fusion barrier, the quantum mechanical effects of tunneling are negligible, and a classical description of overcoming a single "fusion barrier" is sufficient. However, at bombarding energies around and below the fusion barrier, quantum mechanical tunneling plays a crucial role and becomes the primary process contributing to fusion.[1]

The Hill-Wheeler formula for barrier penetration [2] is commonly employed to calculate fusion at energies around the barrier. Stokstad et al conducted systematic measurements of "fusion cross-sections" for the reactions involving ^{16}O on Sm isotopes targets [3, 4] at energies near the conventional Coulomb barrier. Surprisingly, they discovered that the fusion cross-sections were significantly higher, by several orders of magnitude, than expected based on a simple barrier penetration model. Subsequently, numerous other research groups also observed this enhancement in fusion cross-sections at energies near the Coulomb barrier [5, 6, 7,], indicating that it is a widespread phenomenon.

To explain this enhancement, it was proposed that fusion encounters a distribution of barriers rather than a single conventional Coulomb barrier [8-14]. This distribution of barriers could arise from various factors, such as the permanent deformation of the target and/or the projectile in a classical sense as well as quantum effects resulting from coupling the fusion channel with other

channels, including inelastic scattering, proton, or neutron transfer, and breakup channel [5], [15-22].

1.2 Fusion: The Key to Life on Earth

Fusion is a process in which a heavier nucleus is formed from the combination of two lighter nuclei through a nuclear reaction. When the lighter nuclei are lighter than ^{56}Fe, the reaction releases energy (exothermal), whereas if they are heavier than ^{56}Fe, the reaction requires energy (endothermic). The primary mechanism that powers stars for approximately 90% of their lifespan is the fusion of hydrogen nuclei into helium, as illustrated in Figure 1.1[23].

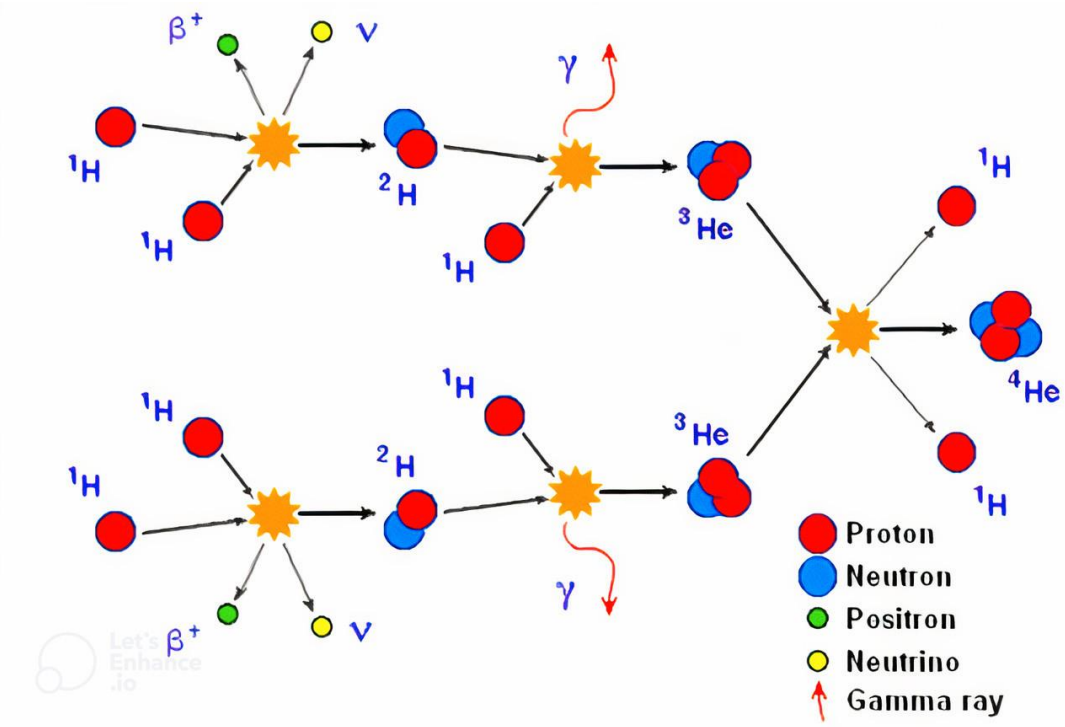

Fig.1.1 Shows the proton-proton chain fusion reaction is produced at 26.7MeV [23]

This occurs naturally within the stellar core, where the immense gravitational pressure facilitates such reactions. Fortunately, the fusion process

is extremely slow due to the minute cross-section of the proton-proton fusion reaction, enabling small stars like the Sun to exist for billions of years. Nuclear fusion also plays a fundamental role in the synthesis of chemical elements throughout the Universe's history.

The abundance of certain elements and isotopes, such as ^{2}H (D), ^{3}He, ^{4}He, ^{6}Li, and ^{7}Li, observed in the Universe can be explained by the Primordial or Big Bang Nucleosynthesis theory. This theory, first introduced in [24,25], describes the generation of heavier elements from protons and neutrons through nuclear reactions that occurred during the initial 1000 seconds after the Big Bang. The production of deuterium (D) from a proton (p) and a neutron (n) was the fundamental process, followed by reactions involving proton-deuterium fusion (p + D) and deuterium-deuterium fusion (D + D or DD), as well as neutron captures and other fusion reactions. However, the expansion of the Universe caused a decrease in density and temperature, halting the synthesis of nuclei heavier than ^{7}Be. [26] in our Universe, including Earth, various elements and isotopes such as ^{12}C, ^{14}N, ^{16}O, ^{28}Si, ^{56}Fe, and ^{197}Au up to ^{238}U exist, among numerous others, owing to the processes mentioned above.

All sources of energy available on Earth, whether directly or indirectly, are derived from nuclear fusion. These sources include solar energy, wind (resulting from temperature and illuminance variations caused by the Sun), waves (related to wind patterns), hydroelectric power (dependent on the water cycle powered by solar energy), biomass and fossil fuels (originating from photosynthesis in plants or the decomposition of organic matter derived from photosynthesis), geothermal energy (stemming from the decay of radionuclides in the Earth's mantle, synthesized through Stellar or Supernovae Nucleosynthesis), and nuclear fission (arising from the induced disintegration of heavy nuclides like ^{235}U, which were synthesized through Supernovae

Nucleosynthesis). or Generating electrical energy through fusion nuclear reactors involves harnessing the power of nuclear fusion reactions to produce electricity and all of this is to reduce global warming phenomena which caught the attention of the world in the last decade. Fusion reactors aim to replicate the same process that powers the stars, such as the Sun, by fusing light atomic nuclei together to form heavier nuclei. This reaction releases an enormous amount of energy.[27,26] The power generated by the Sun, coupled with the specific Earth-Sun distance, creates favorable conditions for life and sustains all forms of life on Earth, including humans. In summary, the existence of the Universe, Earth, and life as we know it heavily relies on nuclear fusion.

1.3 Fusion reaction mechanisms

1.3.1 Direct Complete Fusion (DCF)

Is a process where two atomic nuclei merge together to form a single compound nucleus. This process leads to the complete fusion of the two nuclei without any other reaction channels. The compound nucleus formed in DCF is excited and it relaxes by emitting one or more particles or gamma rays. DCF is the dominant process for heavy-ion fusion reactions at low energies. The mechanism of DCF involves the projectile and the target nucleus approaching each other and overcoming the Coulomb barrier through tunneling. Once the nuclei are close enough, the strong nuclear force takes over and binds the nuclei together to form a compound nucleus. The compound nucleus formed in DCF is excited and it relaxes by emitting one or more particles or gamma rays , as explained in Figure 1.2-a [28, 29].

1.3.2 Sequential Complete Fusion (SCF)

Is a process where the incoming projectile fuses with the target nucleus through a series of two or more compound nuclei . The compound nuclei formed in each step of the process gradually approach the final state through successive

Direct Complete Fusion (DCF) reactions. SCF is the dominant process at high energies where DCF and Non-Capture Breakup (NCBU) cross-sections are negligible. The mechanism of SCF involves the target and the projectile nucleus approaching each other and overcoming the Coulomb barrier through tunneling to form a compound nucleus. The compound nucleus formed in the first step of the process can undergo a second fusion reaction with the remaining part of the projectile to form a heavier compound nucleus. This process can be repeated several times until the final compound nucleus is formed. The compound nuclei formed in each step of the process gradually approach the final state through successive DCF reactions , as explained in Figure 1.2-b [28, 29].

1.3.3 Incomplete Fusion (ICF):

Incomplete fusion refers to a nuclear reaction in which only a fraction of the colliding nuclei merge together to form a compound nucleus, while some nucleons are not fully captured. In ICF, the interacting nuclei approach each other and experience nuclear forces but fail to overcome the entire Coulomb barrier and fully merge. Instead of complete fusion, some nucleons from the colliding nuclei are left behind, leading to the formation of intermediate reaction products. ICF is influenced by various factors, including the incident energy, the structure and stability of the colliding nuclei, and the reaction dynamics. It can result in the production of exotic nuclei and can significantly affect the properties of the compound nucleus formed in the reaction, as explained in Figure 1.2-b.[30]

1.3.4 Non-Capture Breakup (NCBU)

Is a process in which the incoming projectile breaks up into two or more fragments before reaching the target nuclei. This process occurs when the energy of the projectile is insufficient to overcome the Coulomb barrier of the

target nucleus, but is sufficient to break it up. NCBU is a significant reaction channel at intermediate energies. The mechanism of NCBU involves the projectile and the target nucleus approaching each other and interacting through the Coulomb and nuclear forces. If the projectile energy is not sufficient to overcome the Coulomb barrier of the target nuclei but is sufficient to break it up, the projectile breaks up into two or more fragments before reaching the target nucleus. The fragments then interact with the target nucleus separately, leading to a more complex reaction product, as explained in Figure 1.2-b.[31]

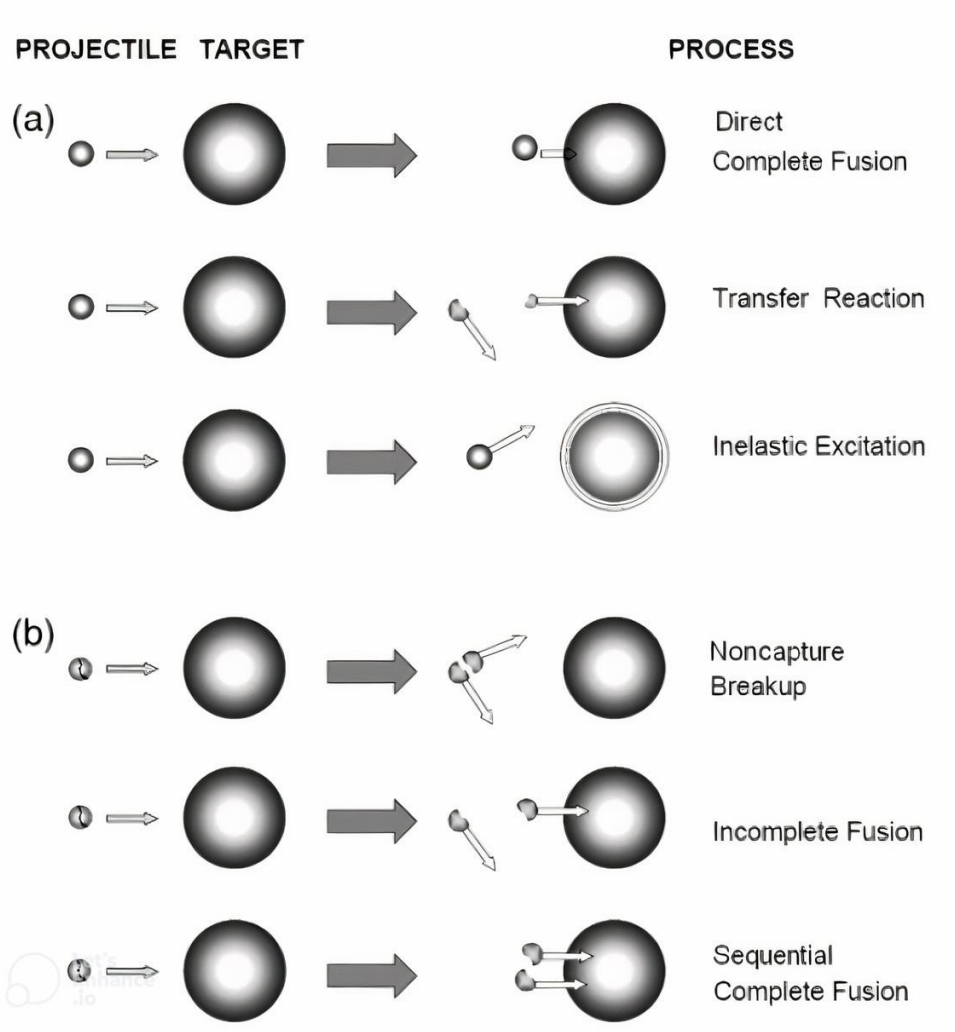

Fig.1.2 Illustrative diagrams of reaction mechanisms (a) any kind of nuclei are included (b) only weakly bound nuclei are included [32]

1.4 Literature Review

In 1980, Beckerman *et al.* [33] during the investigation of the fusion of $^{58}Ni + ^{64}Ni$ at Q+2n = 3.9MeV, the impact of positive Q-value neutron transfer (PQNT) channels was first noticed on near-barrier fusion cross sections. They directly compared the fusion excitation functions of $^{58,64}Ni + ^{58,64}Ni$ in an experiment, with the symbol "+" notation representing the absorption of neutrons from the target nuclei.

In 1983, Broglia *et al.* [34] they did a vital study to check the results of Beckerman's studies on the system $^{58}Ni + ^{64}Ni$ and find out that the sub-barrier enhancement of fusion observed in $^{58}Ni + ^{64}Ni$ is due to a kinematic effect caused by the transfer of two neutrons during the fusion process, which reduces the neutron transfer cross-section.

In 1992 N. Rowley *et al.* [35] they found an important result that the broad distributions of experimental fusion cross-sections are produced by sequential neutron transfers. Neutron flow may result from the development of a neck between the projectile and target as a result of a collision with a finite Q-value.

In 1998 H. Timmers *et al.* [36] they studied two systems $^{40}Ca+^{90}Zr$ and $^{40}Ca+^{96}Zr$ and found that the distributions barrier of the two systems, are distinctively different. Below 95 MeV, no additional barriers are present in the reaction $^{40}Ca + ^{90}Zr$, whereas, for $^{40}Ca + ^{96}Zr$, three additional barriers exist. This marks an important difference between the two systems. the lighter system is well described by coupled-channels calculations including multi-phonon excitations, this coupling scheme fails completely for the heavier system. The possible reason for these differences in the barrier distributions between the lighter and heavier systems is attributed to the strong coupling to multi-neutron transfer in the $^{40}Ca + ^{96}Zr$ system. The simplified coupled-channels calculations

suggest that the neutron transfer proceeds sequentially and forms a neck between the projectile and the target. this could act as fusion's "doorway state". This intermediate state lowers the barrier and makes the fusion process easier at energies below the barrier, significantly increasing fusion cross-sections.

In 2000, V.Yu. Denisov. [37] Conducted a study on a number of different systems using the CCFUS code and concluded that it is noteworthy that the fusion cross sections for the $^{24}O+^{58}Ni$ and $^{40}Ca+^{96}Zr$ systems display different patterns in the vicinity of the barrier due to the contribution of the one-neutron transfer channel. While this channel has negligible impact on the $^{40}Ca+^{96}Zr$ reaction, it plays a significant role in the $^{24}O+^{58}Ni$ reaction. This discrepancy can be attributed to the distinct one-neutron transfer channel's Q-values, which are Q1n = 5.29 MeV and Q1n = 0.508 MeV for $^{24}O+^{58}Ni$ and $^{40}Ca+^{96}Zr$, respectively.

In 2003, V. I. Zagrebaev. [38] Conducted an analytical study of many systems: $^{40}Ca+^{48}Ca$, $^{48}Ca+^{48}Ca$, $^{40}Ca+^{96}Zr$, $^{42}Ca+^{46}Ca$, $^{44}Ca+^{44}Ca$, $^{18}O+^{58}Ni$, $^{16}O+^{60}Ni$, $^{6}He+^{209}Bi$, $^{4}He+^{209}Bi$, and $^{6}He+^{238}U$, It was found that neutron transfer with negative Q values does not lead to an increase in combinatorial energy at energies near or below the slit based on the analysis of fusion cross-sections.in reactions with negative values of all Q-value, there is no additional enhancement of the total penetration probability of the Coulomb barrier due to neutron transfer in the entrance channel. This is because the "partial" penetration probability becomes smaller for negative Q values.

In 2004, Angela Bonaccorso *et al*.[39] they highlighted the possibility of forming strongly bound nuclei through The transfer or pick-up of neutron or proton can have a significant effect on the fusion reaction cross-section. In particular, the transfer of nucleons can lead to the formation of a compound

nucleus that is more strongly bound than the original target and projectile nuclei, which can enhance the probability of fusion. This effect is known as the "compound nucleus" mechanism. in the case of the $^{16}O + ^{208}Pb$ system, it has been shown that the transfer of up to four neutrons can significantly enhance the fusion cross-section at energies near and below the Coulomb barrier Similarly, in the case of the $^{58}Ni + ^{208}Pb$ system, the transfer of up to six neutrons and four protons has been observed.

In 2006, C. Simenel *et al*.[40] did a study and found that the different orientations of the deformed nucleus during the fusion process can affect the reaction paths and fusion probability around the barrier. A study using the Time-Dependent Hartree-Fock theory with a full Skyrme force investigated the role of deformation on fusion probability. The study found that considering all possible orientations leads to a distribution of fusion probabilities due to the coupling between static deformation and relative motion. Long-range Coulomb coupling was shown to reduce fusion probability, and the study was used to interpret the hindrance of near-barrier fusion in coupling channel calculations with the code CCFULL.

In 2007, B. K. Nayak *et al*. [41] they did a study and found that the experimental barrier distributions for $^{28}Si+^{115}In$ and $^{30}Si+^{115}In$ systems can affect the fusion process in two ways due to the oblate and prolate deformed nuclei of ^{28}Si and ^{30}Si, and those two ways are : (i) The fusion barrier height depends on the orientation of the deformation axis of the projectile with the collision axis, thereby giving rise to a distribution of barriers rather than a single barrier as in the case of a spherical target and projectile, (ii) The barrier distribution is also affected due to reorientation of the deformed ^{28}Si and ^{30}Si projectiles before fusion in the Coulomb field of the target nuclei similar to that predicted for $^{24}Mg+^{208}Pb$ system as reported From the quantum mechanical

point of view, the reorientation is a consequence of the excitation of rotational states. In the case of coupling of rotational states of the target/projectile to the fusion channel, the coupling matrix elements consist of both nuclear and Coulomb parts.

In 2011, V. V. Sargsyan *et al*.[42] did a study by using the quantum diffusion approach which was applied to study the capture process in the reactions with deformed and spherical nuclei at sub-barrier energies. The available experimental data at energies above and below the V_b are well described. As shown, the experimentally observed sub-barrier fusion enhancement is mainly related to the quadrupole deformation of the colliding nuclei and neutron transfer with the positive Q value. The change of the magnitude of the capture cross-section after the neutron transfer occurs because of the change of the deformations of nuclei, when after the neutron transfer the deformations of nuclei do not change or decrease, the neutron transfer weakly influences or suppresses the capture process.

In 2012, V. V. Sargsyan *et al* [43].they studied the role of neutron transfer with positive Q-value in sub-barrier capture reactions ^{132}Sn,^{130}Te+^{58,64}Ni, and ^{60}Ni+^{100}Mo. It is shown that the transfer of two neutrons influences the sub-barrier capture through the change of the deformations of the colliding nuclei. Based on our analysis, one can understand why the influence of neutron transfer is strong in some capture reactions but weak in others.

In 2014, G. L. Zhang *et al* [44]. they did a study by using a universal fusion function approach to analyze the effects of (PQNT) on the fusion process in various systems. They found that significant deformation of the interacting nuclei following neutron transfer is crucial for strong sub-barrier fusion enhancement due to the (PQNT). In contrast, if the deformation of the nuclei is

minimal or decreases after neutron transfer, these channels have little effect on the fusion cross-sections.

In 2015, Falah K. Ahmed *et al.* [45] they did a study investigating the effect of breakup on the σ_{fus} of weakly bound nuclei. The study focuses on the fusion of ^{9}Be with ^{208}Pb. The researchers employ a Coupled-Channel approach to accurately calculate σ_{fus}, taking into account the coupling to the breakup channel .to perform the calculations, utilizing a program called "CCFULL". The results obtained from the study reveal the significance of including the breakup channel in calculations of fusion cross sections for weakly bound nuclei. The experimental data are compared to the calculated results. It is observed that the inclusion of the breakup channel in the calculations leads to a better agreement between the theoretical predictions and the experimental data. This highlights the importance of considering the breakup channel in order to accurately describe the fusion process for weakly bound nuclei.

In 2016, Fouad A. Majeed *et al*. [46] they did a study focusing on the semi-classical treatment of fusion and breakup processes of ^{6,8} He halo nuclei on target ^{238}U. The study aims to investigate the effect of channel coupling on fusion reaction cross-sections and fusion barrier distributions for these systems. to achieve this, a semi-classical approach is employed. the calculations are performed using the program SCF code for semi-classical calculation and CCFULL code for quantum mechanical calculation It is observed that the inclusion of breakup states channels significantly affects the fusion reaction cross-sections and fusion barrier distributions. The coupling between these channels and the fusion process leads to enhanced fusion probabilities and modifies the shape of the fusion barrier distribution.

In 2017, F.A. Majeed *et al* .[47] they did investigate the impact of coupled-

channel calculations on (σ_{fus}) and (D_{fus}) for the $^{46}Ti+^{46}Ti$ and $^{58}Ni+^{58}Ni$ systems using a semi-classical method. They compared the results of the semi-classical approach to those of the full quantum mechanical calculations made with the "CCFULL code" which included all order coupling, and also to available experimental data. Their findings indicated that the semi-classical calculations were more consistent with the experimental data than the calculations of the full quantum mechanical when both the cases of no coupling and coupling effects were considered.

In 2017, F.A. Majeed *et al* .[48] They conducted a study to investigate the couple channel effect, in which they utilized both semi-classical and quantum mechanical methods to examine the probability of reaction, as well as the σ_{fus} and D_{fus}, for the systems $'He+^{233}U$, $^{13}C+^{48}Ti$. To carry out their investigation, they employed SCF and CC codes for the semi-classical and quantum approaches, respectively. The outcomes of their calculations revealed a high level of consistency between their findings and the experimental data that was available for these systems.

In 2019, Fatima M. Hussian *et al*.[49] a study in which they employed both semi-classical and quantum mechanical methods to compute the σ_{fus} ,D_{fus} and P_{fus} for the systems ^{40} $Ar+^{144,148,154}Sm$. To perform their calculations, they used SCF and CCFULL computer codes for the semi-classical and quantum approaches, respectively. In the semi-classical calculations, they employed the (CDCC). For the first two systems, they adopted coupling with vibrational excitation using (1 and 2) phonons and 1 phonon for (Ar and $^{144,148}Sm$), respectively. Meanwhile, for the $Ar+^{154}Sm$ system, they considered coupling to rotational levels for Sm, and they treated the projectile as inert in the quantum calculations. The results of their investigation demonstrated the compatibility of the semi-classical model with the available data.

In 2020, Fatima M. Hussian *et al*. [50] they did a study on the fusion reactions of systems that involve halo nuclei, such as $^{8}B+^{58}Ni$, $^{11}Be+^{209}Bi$, and $^{15}C+^{232}Th$, which were investigated using two- and multi-coupled channel calculations. The (CDCC) method was used to account for the coupling between the breakup and elastic channels in both the full quantum and semi-classical approaches. The calculations of (σ_{fus}), (D_{fus}), and (P_{fus}) closely reproduced the measured data for the studied systems above and below V_b. However, when it comes to two-channel coupling in both semi-classical and quantum mechanical approaches, the measured data above V_b were overestimated.

In 2020, Malik S. Mehemed *et al.* [51] they did a study that aims to explore the application of the semi-classical and quantum mechanical approach, based on the Winther and Alder theory that describes Coulomb excitation. The study utilized (CCCD) approach, which enabled the examination of the channel coupling effects on the determination of (σ_{fus}) and (D_{fus}) for the systems $^{14}N+^{59}Co$, $^{16}O+^{64}Ni$, and $^{18}O+^{64}Ni$. Both the semi-classical and quantum models were employed in the investigation. A comparison between the results of the two models, as well as the corresponding experimental data, revealed that the adopted semi-classical model was highly competitive with the quantum mechanical model. Overall, this approach was found to be an efficient and effective means of studying the properties of fusion reactions.

In 2021, Maryam H. Abd Madhi *et al* .[52] they did a study that states that a semi-classical approach was utilized to compute (σ_{fus}), (D_{fus}), and (P_{fus}) for systems that involve halo nuclei, specifically $^{6}He+^{64}Zn$, $^{8}B+^{58}Ni$, and $^{8}He+^{197}Au$. The semi-classical and quantum mechanics treatments involved the use of the WKB approximation, and (CDCC) method to. The findings of the semi-classical calculations were compared to available experimental data, as well as quantum mechanics calculations. The results indicated that the quantum

mechanics coupled channels were very similar for σ_{fus} below and above the (V_b), in accordance with the experimental results.

In 2022, Shaimaa A. Abbas *et al*. [53] they did a study on the fusion reactions that involve neutron or proton-rich halo nuclei, and the coupling mechanism between the elastic and breakup channels poses a significant challenge. The objective of this study was to estimate the best coupling parameter for introducing the effect of coupled-channels into the calculations of (σ_{fus}), (D_{fus}), and the average angular momentum ($\langle L \rangle$) for the following systems: $^{6}He+^{206}Pb$, $^{8}B+^{28}Si$, $^{11}Be+^{209}Bi$, $^{17}F+^{208}Pb$, $^{6}He+^{238}U$, $^{8}He+^{197}Au$, and $^{15}C+^{232}Th$, using a quantum mechanical approach. To carry out this investigation, quantum Coupled-Channel Calculations were conducted using CC code. The predictions of the quantum mechanical approach were found to be comparable to the available measured data. Furthermore, a comparison of the theoretical calculations of quantum mechanics with the relevant measured data demonstrated good agreement both above and below the V_b.

In 2023, Wendi Chen *et al* [54]. Did a research that investigates the behavior of weakly bound nucleus ^{6}Li in fusion reactions with various targets ^{28}Si, ^{64}Ni, ^{144}Sm, and ^{209}Bi at energies around the V_b. They used the (CDCC) method which takes into account the coupling between the projectile, target, and relative motion. They demonstrate the importance of including closed channels, which have negative energies, for accurate calculations. They found that the CDCC method provides a good description of the experimental data for σ_{fus}, and that closed channels play a crucial role in improving the description of partial wave fusion cross sections. They also compare their results to those obtained with the sum-rule model and find good agreement.

1.5Aim of the study

This study aims to show the impact of adding the channel coupling between the elastic channel and the breakup channel to study the fusion reaction properties, and its effect on calculations of the cross-section, total fusion σ_{fus}, fusion barrier distribution D_{fus}, and fusion probability P_{fus} by using both the semi-classical and quantum mechanical approach for the systems ^{28}Si+^{90}Zr, ^{28}Si+^{92}Zr, ^{28}Si+^{94}Zr, ^{28}Si+^{96}Zr, ^{32}S+^{90}Zr, ^{32}S+^{96}Zr, ^{35}Cl+^{92}Zr, ^{41}K+ ^{28}Si, ^{45}K+ ^{28}Si, ^{44}Ar+^{28}Si, ^{41}K+^{16}O that involving one neutron or one proton transfer reactions. And comparing the results with the measured experimental data.

Chapter Two

Theoretical Background

2.1 Introduction

The fusion of light-stable nuclei can be adequately described by simple barrier penetration models. However, for heavier and more exotic systems, especially at energies below the barrier, these models consistently underestimate the fusion cross-section. This is due to the fact that these models assume that the fusing nuclei are rigid objects that interact only elastically, with the only variable being the nuclear separation distance. In reality, the fusing nuclei are complex objects that can follow non-elastic channels such as breakup and transfer during the fusion process. In a static fusion model, the fusing nuclei are considered to be frozen in their ground state configurations. However, at energies near the barrier, when the two nuclei approach each other adiabatically, single-particle excitations and particle transfers can play a significant role prior to fusion [55,56]. In this section, we introduce a formulation for the theory and equations that are used in the calculations and their effect on the fusion reaction. Specifically, we investigate the collision of two nuclei in the presence of coupling between the relative motion of the colliding nuclei's centers of mass and a nuclear intrinsic motion.

2.2 Semi-classical treatment

Quantum mechanics employs three approximate methods, namely perturbation theory, variational method, and semi-classical approximation. Perturbation theory produces a series expansion for quantities of interest, while the variational method allows the best estimate from a trial solution. On the other hand, the semi-classical approximation supposes that h is small compared to the action function in the corresponding classical problem. One of the most commonly used approximations is the Wentzel-Kramers-Brillouin (WKB)[57,58,59] method, which was independently introduced by Wentzel, Kramers, and Brillouin at the advent of quantum mechanics. In the UK, the

same approximation is known as the Jeffreys-Wentzel-Kramers-Brillouin (JWKB), where the "J" stands for Jeffreys [60]. The JWKB is a semi-classical approximation invented in the 19th century and applied to the Schrödinger equation. Despite being an age-old approximation, the WKB method still remains an area of interest, both conceptually and practically.

In the Schrödinger equation [60],

$$\left(\frac{\mathrm{d}^2\psi(r)}{\mathrm{dr}^2} + k^2(r)\psi(r) \right) = 0 \qquad 2.1$$

Where,

$$k(r) = \frac{1}{\hbar}[2\mu(E - V(r))]^{1/2} \qquad 2.2$$

According to [59], the phase-amplitude form can be used to express the wave function $\psi(r)$.

$$\psi(r) = A(r)e^{i\frac{Q(r)}{\hbar}} \qquad 2.3$$

If the potential is considered a constant, the wave function can be denoted as a plane wave, Q(r) = $\hbar$k(r), where A(r) is the amplitude of the wave function. When the potential varies slowly in space, the action Q(r) is expected to increase at a rate of δQ(r) = $\hbar$k(r)dr, while the amplitude A(r) varies more slowly than Q(r). The amplitude A(r) can be incorporated into the exponent as the imaginary part of Q(r). In the classical limit where $\hbar \to 0$, Dunham's work [61] is followed, and it can be assumed that Q(r) can be expressed as a convergent (or at least asymptotic) series in powers of $\hbar$ as shown below [62].

$$Q(r) = \sum_n \frac{\hbar^n}{n!} Q_n(r) = Q_0(r) + \hbar Q_1(r) + \frac{\hbar^2}{2} Q_2(r) + \cdots \qquad 2.4$$

By inserting equations 2.3 and 2.4 into the Schrödinger equation (2.1) and rearranging it in powers of $\hbar$, one can obtain the following expression (up to second order in $\hbar$) [63].

$$\frac{1}{2\mu}\left(\frac{dQ_0}{dr}\right)^2 + \left(E - V(r)\right) + \frac{\hbar}{\mu}\left(\frac{dQ_0}{dr}\frac{dQ_1}{dr} - \frac{i}{2}\frac{d^2Q_0}{dr^2}\right) + \frac{\hbar^2}{2\mu}\left(\frac{dQ_0}{dr}\frac{dQ_2}{dr} + \left(\frac{d^2Q_1}{dr}\right)^2 - i\frac{d^2Q_1}{dr^2}\right) + \cdots = 0 \quad 2.5$$

In order for the wave equation to hold true regardless of the value of $\hbar$, the coefficient of each power of $\hbar$ must be zero. As a result, a series of equations can be obtained [64].

$$\frac{1}{2\mu}\left(\frac{dQ_0}{dr}\right)^2 + \left(E - V(r)\right) = 0 \quad 2.6$$

$$\left(\frac{dQ_0}{dr}\frac{dQ_1}{dr} - \frac{i}{2}\frac{d^2Q_0}{dr^2}\right) = 0 \quad 2.7$$

$$\left(\frac{dQ_0}{dr}\frac{dQ_2}{dr} + \left(\frac{d^2Q_1}{dr}\right)^2 - i\frac{d^2Q_1}{dr^2}\right) = 0 \quad 2.8$$

By solving equations above we get [61],

$$Q_0 = \mp\int\sqrt{2\mu\left(E - V(r)\right)}dr = \mp\int \hbar\mathrm{k(r)}dr \quad 2.9$$

And,

$$Q_1 = \frac{i}{2}ln\left[\frac{dQ_0}{dr}\right] \quad 2.10$$

Also,

$$Q_2 = \frac{\mu}{2}\frac{1}{(\hbar\mathrm{k})^3}\frac{dV}{dr} + \frac{\mu^2}{4}\int\frac{1}{(\hbar\mathrm{k})^5}\left(\frac{dV}{dr}\right)^2 dr \quad 2.11$$

In general, Q_1 cannot be considered negligible compared to Q_o, but Q_2 can be assumed to be small if $\frac{dV}{dr}$ is small and E-V(r) is non-zero, that is, not in the vicinity of a classical turning point.

The lowest order WKB approximation (LO-WKB) disregards the terms that contain Q_n with $n \geq 2$ in the phase of the wave function. Thus, the validity of the lowest-order WKB can be determined using the following criterion [61].

$$\frac{\mu}{\hbar^2 k^3(r)} \frac{dV}{dr} \ll 1 \qquad 2.12$$

Thus, the WKB method is suitable for slowly changing potentials in regions that are far from classical turning points. By retaining only Q_o and Q_1 in Equation 2.4, the approximate wave function for the lowest order WKB (L.0-WKB) is obtained [63].

$$\psi^{WKB}(r) = \frac{A}{\sqrt{k(r)}} exp\left(i \int_b^r k(r)dr\right) + \frac{B}{\sqrt{k(r)}} exp\left(i \int_r^b k(r)dr\right) \qquad 2.13$$

Here, "b" represents an arbitrary point that solely influences the normalization factors A and B. Within the classically forbidden region, where V(r) > E, the wave number $K(r) \rightarrow ik(r)$ is imaginary, and the ψ^{WKB} (r) varies exponentially. Conversely, within the classically allowed region, the WKB wave function oscillates.

Fig. 2.1 and Eqn. 2.13 demonstrate that the WKB approximation is not suitable in the vicinity of a turning point, where r = b and V(b) = E, since the condition for WKB applicability (Eqn. 2.12) breaks down in this region, causing the amplitude of the WKB wave function to diverge. Consequently, the primary challenge in WKB is to connect the sinusoidal solution in the allowed zone to

the exponential-type solution in the adjacent, classically forbidden zone across a classical turning point.

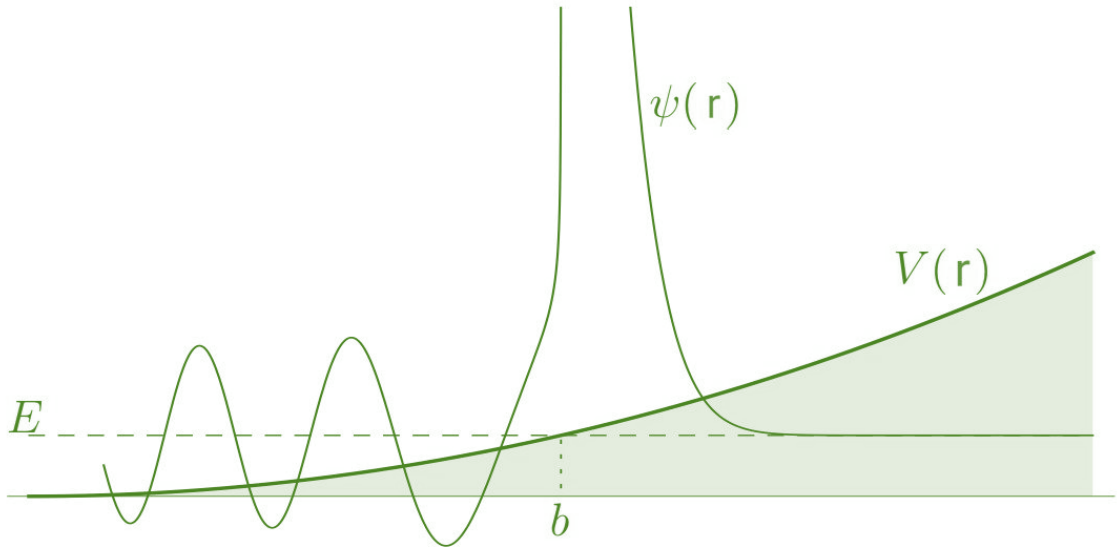

Figure 2.1 depicts a schematic representation of the WKB wave function, which is sinusoidal in the allowed zone and decays in the forbidden zone. However, near the turning point, b [65], the WKB wave function diverges.

In most cases, when the potential is sufficiently close to a turning point, it can be approximated as a straight line. In such scenarios, the Schrödinger equation has a solution represented by the Airy function, which can be expressed in terms of Bessel functions with order 1/3 [63]. When the WKB approximation is valid, and the Airy function's form is asymptotic, a smooth connection between the two can be established. This allows the constants A and B in Equation 2.13 on the classically allowed side to be related to the coefficients of the two exponentially varying waves on the forbidden side. Figure 2.2 illustrates how four connection formulae can be utilized to connect sinusoidal wave functions to exponential ones and vice versa.

Case 1: the turning point on the left of the barrier

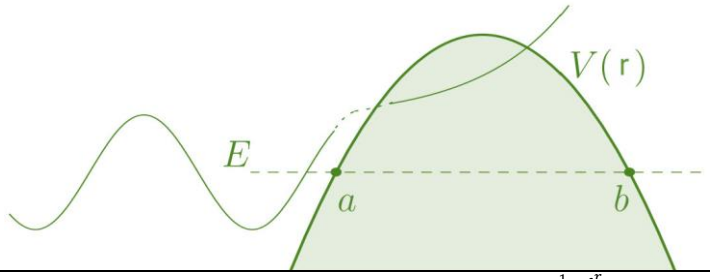

$$\frac{-1}{\sqrt{k(r)}}sin\left(\int_r^a k(r)dr-\frac{\pi}{4}\right)=\frac{-1}{\sqrt{k(r)}}cos\left(\int_r^a k(r)dr+\frac{\pi}{4}\right)\leftrightarrows e^{\frac{1}{\sqrt{k(r)}}\int_a^r k(r)dr}$$

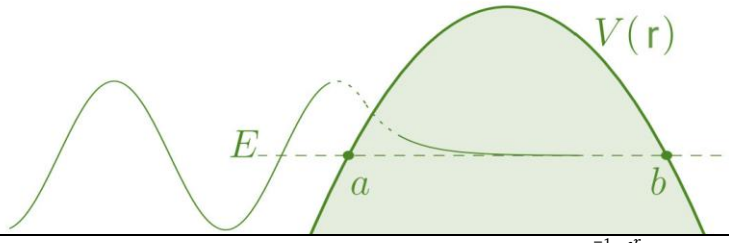

$$\frac{1}{\sqrt{k(r)}}cos\left(\int_r^a k(r)dr-\frac{\pi}{4}\right)=\frac{1}{\sqrt{k(r)}}sin\left(\int_r^a k(r)dr+\frac{\pi}{4}\right)\leftrightarrows e^{2\frac{-1}{\sqrt{k(r)}}\int_a^r k(r)dr}$$

Case 2: the turning point on the right of the barrier

$$e^{2\frac{-1}{\sqrt{k(r)}}\int_r^b k(r)dr}\leftrightarrows\frac{1}{\sqrt{k(r)}}cos\left(\int_b^r k(r)dr-\frac{\pi}{4}\right)=\frac{1}{\sqrt{k(r)}}sin\left(\int_b^r k(r)dr+\frac{\pi}{4}\right)$$

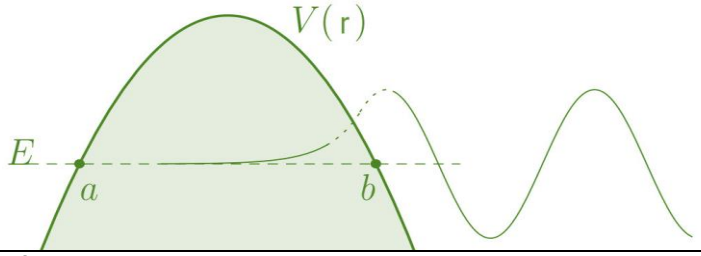

$$e^{\frac{1}{\sqrt{k(r)}}\int_r^b k(r)dr}\leftrightarrows\frac{-1}{\sqrt{k(r)}}sin\left(\int_b^r k(r)dr-\frac{\pi}{4}\right)=\frac{1}{\sqrt{k(r)}}cos\left(\int_b^r k(r)dr+\frac{\pi}{4}\right)$$

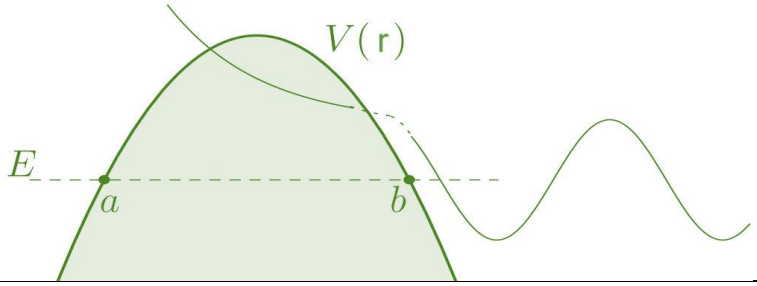

Fig.2.2 explaining the formulae of the two connection in two cases [65]

2.3 Quantum mechanical treatment

One conventional method of reducing the impact of coupling between intrinsic degrees of freedom and relative motion in fusion is to solve coupled channel equations that consider all related channels. In the past, coupled-channel calculations commonly used the linear coupling approximation, which involved expanding the coupling potential in deformation parameter powers and retaining only the linear expression. However, it has been shown that non-linear couplings have a significant impact on the shapes of fusion barrier distributions, and the linear coupling approximation is not as accurate as new high-quality fusion cross-section results [66,67]. To analyze direct nuclear interactions, the CDCC approach, which includes the breakup of roughly bound particles such as deuterons, ^{6,7}Li, and ^{13}C, was used. CDCC is an extension of the conventional CC approach for bound clusters, and its goal and principal assumptions are similar to those of conventional Coupled Channels. CDCC calculates experimentally observable quantities such as analyzing powers and cross-sections to compare with experimental data. A CDCC calculation typically starts by adopting models of the multi-step direct process and identifying how channels are coupled to each other. In this work, we assume that the model includes only two channels, either a bound or an unbound state, and that only one channel may be in an unbound state that can be well approximated by a state of interacting two nucleons or two fragments each in a definite bound state [67].

2.3.1 No-coupling or one-channel description

The simplest quantum mechanical method for evaluating elastic and cross-section reactions is single-channel calculations. The total angular momentum J can be used to replace the angular momentum of the relative motion in each

channel [68,69]. to a good approximation. This approximation is also known as the iso-centrifugal or no-Coriolis approximation, and it is used in this software. The equations used for single-channel (no-coupling) are denoted as Eqs. [70].

$$\left(-\frac{\hbar^2}{2\mu}\frac{\mathrm{d}^2}{\mathrm{dr}^2}+\frac{\hbar^2 J(J+1)}{2\mu \mathrm{r}^2}+V_N^{(0)}(r)+\frac{Z_P Z_T e^2}{\mathrm{r}}\right)\psi(r)=E\,\psi(r) \qquad 2.14$$

In this context, the radial component of the relative motion coordinate is represented by r, and the reduced mass is μ. The bombarding energy in the center of the mass frame is denoted as E. The nuclear potential in entrance channels is represented by $V_N^{(0)}$ In this software, the Woods-Saxon parametrization is used to represent the nuclear potential, [70, 71].

$$V_N(r)=\frac{-V_0}{1+\exp\left[\frac{r-R_n}{a_0}\right]} \qquad 2.15$$

The depth of the potential is represented by V_o, while a_0 represents the potential diffuseness. The nuclear potential's radius, denoted by R_n, is determined using the equation provided [70].

$$R_n=r_0\left(A_P^{1/3}+A_T^{1/3}\right) \qquad 2.16$$

In this context, the radius parameter is represented by r_o.

To solve the equations of single-channel, boundary conditions were imposed such that incoming waves were present only at $r = r_{min}$, and outgoing waves were present at infinity for each channel except for entrance channels (n = 0), which had incoming waves with amplitude one. This boundary condition is referred to as the incoming wave boundary condition (IWBC) [72], and is suitable for medium-light interactions where strong absorption occurs within the Coulomb barrier. The software CC uses the Coulomb pocket's minimum

location within the barrier as r_{rim}. At a finite distance r_{max}, where both the Coulomb coupling and the nuclear potential were sufficiently weak, the numerical solution was matched to a linear combination of outgoing and incoming functions of Coulomb wave. The boundary conditions are expressed as below [70,71].

$$\psi(r) \rightarrow Texp\left[-i \int_{r_{min}}^{r} k(\acute{r})\, d\acute{r}\right], r \leq r_{min} \qquad 2.17$$

The formula of k(r) is

$$\mathrm{k(r)} = \left[\frac{2\mu}{\hbar^2}\left(E - \frac{\hbar^2 J(J+1)}{2\mu \mathrm{r}^2} - V_n^{(0)}(r) - \frac{Z_P Z_T e^2}{\mathrm{r}}\right)\right]^{1/2} \qquad 2.18$$

To ensure that only incoming waves were present at $r \rightarrow r_{min}$, the software CC solved the single-channel equations outward from r_{min}.

Our focus is primarily on the comprehensive process, where the inherent degree of freedom appears in every last state. The inclusive penetrability is obtained by adding all possible intrinsic states together, as described below [70,71].

$$P_J(E) = \sum \frac{k(r_{\min})}{k_0} |T|^2 \qquad 2.19$$

The average angular momentum of the compound nucleus and the fusion cross-section are computed using the equations provided below [70].

$$\sigma_{Fus}(E) = \sum_J \sigma_J(E) = \frac{\pi}{k_0} \sum_J (2J+1) P_J(E) \qquad 2.20$$

2.3.2 Couple channel description:

In addition to considering the relative motion between colliding nuclei, a common theoretical method explicitly deals with the nuclear intrinsic degrees of freedom [66]. In this approach, the reaction is described using the total wave function $\psi(\vec{r},\xi)$, where ξ represents the set of intrinsic coordinates of the projectile and target nuclei, and $\vec{r}$ represents the separation vector of the colliding nuclei. The dynamics of this reaction are determined using the Hamiltonian equation, as explained [73],

$$H = H_0 + T + U \qquad 2.21$$

In this context, $H_0 \equiv H_0(\xi, P_\xi)$ represents the intrinsic Hamiltonian, while $T = \frac{-\hbar^2\nabla^2}{2\mu}$ is the kinetic energy operator used to calculate the relative motion between the target and projectile nuclei. $U \equiv \mathrm{U}(\vec{r},\xi)$ represents the interaction potential between the nuclei. The eigenstates of the intrinsic Hamiltonian are denoted by$|\beta\rangle$ and correspond to the solutions of the Schrödinger equation, as explained below [73].

$$(e_\beta - H_0)|\beta\rangle = 0 \qquad 2.22$$

the orthonormality is,

$$\langle\acute{\beta}|\beta\rangle = \int \psi^*_{\acute{\beta}}(\xi)\,\psi_\beta(\xi)\,d\xi = \delta_{\beta\acute{\beta}} \qquad 2.23$$

In this context, the wave function $\psi_\beta(\xi)\left(\psi^*_{\acute{\beta}}(\xi)\right)$ correspond to the case $|\beta\rangle(|\beta\rangle)$ in the ξ representation. The interaction potential can be split as described below [73]

$$U = U' + U'' \qquad 2.24$$

The diagonal in channel space is U'

$$U' = \sum_{\beta} |\beta\rangle\, U'_{\beta}\, \langle\beta\,| \qquad 2.25$$

Where

$$U'' = \sum_{\beta} |\beta\rangle\, U''_{\beta,\beta'}\, \langle\beta'| \qquad 2.26$$

$$U'_{\beta}(\vec{r}) = \int d\xi\, \left|\psi_{\beta}(\xi)\right|^{2}\, U'(\vec{r},\xi) \qquad 2.27$$

$$U''_{\beta,\beta'}(\vec{r}) = \int d\xi\ \psi^{*}_{\beta}(\xi)\, U''(\vec{r},\xi)\psi_{\beta}(\xi) \qquad 2.28$$

The potential U' is an estimate, except for the channel space where it is diagonal. Once U' is selected, U" can be determined using the relation $U'' = U - U'$. It is often preferred to choose U' such that U" is completely off-diagonal. In such cases, the components of U" can be described, as stated in below [73].

$$U''_{\beta,\beta'}(\vec{r}) = \int d\xi\ \psi^{*}_{\beta}(\xi)\, U''(\vec{r},\xi)\psi_{\beta}(\xi) - \delta_{\beta\beta}\, U'_{\beta}(\vec{r}) \qquad 2.29$$

The equations of a coupled channel can be derived from the Schrödinger equation, as explained [73].

$$(E - H)\, |\psi_{\beta}(\beta_0\, \overrightarrow{k_0})\rangle = 0 \qquad 2.30$$

And the channel expansion would be :

$$|\psi_{\beta}(\beta_0\, \overrightarrow{k_0})\rangle = \sum_{\beta} |\psi_{\beta}(\beta_0\, \overrightarrow{k_0})\rangle\ |\beta\rangle \qquad 2.31$$

In this context, the notation $|\psi_\beta(\beta_0\ \overrightarrow{k_0})\rangle$refers to a collision that begins in channel β_0 with $\overrightarrow{k_0}$ as the wave vector, and the energy scale is chosen such that (e_{β_0} =0). Due to the off-diagonal part of the reaction, the solution of the Schrödinger equation has components $|\psi_\beta(\beta_0\ \overrightarrow{k_0})\rangle$ for both $\beta = \beta_0$ and $\beta \neq \beta_0$. The infinite expansion of Equation 2.24 is truncated to include only the most relevant channels, or closed coupling approximation. To account for the loss of flux through the neglected channels, one may include the imaginary part in channel potentials $U'_\beta(\vec{r})$. To determine the wave function, the Hamiltonian equation must be written as below [73].

$$H = H_0 + H' + U'' \qquad 2.32$$

where

$$H' = T + U' \qquad 2.33$$

By substituting equations 2.31 and 2.32 into equation 2.30 and taking the numeric product with all intrinsic states $|\beta\rangle$), one can obtain the equations of coupled channels, as decsribed below [74].

$$(E_\beta - H'_\beta)\,|\psi_\beta(\beta_0\ \overrightarrow{k_0})\rangle = \sum_{\beta'} U''_{\beta,\beta'}(\vec{r})|\psi_{\beta'}(\beta_0\ \overrightarrow{k_0})\rangle \qquad 2.34$$

Or,

$$\left[E_\beta + \frac{\hbar^2\Delta}{2\mu} - U'_\beta(\vec{r})\right]\psi_\beta(\vec{r}) = \sum_{\beta'} U''_{\beta,\beta'}(\vec{r})\psi_{\beta'}(\vec{r}) \qquad 2.35$$

Where

$$E_\beta = E - e_\beta \qquad 2.36$$

For example, the total energy of the relative motion in channel β can be expressed as follows:

$$H'_\beta = T + U'_\beta \qquad 2.37$$

Equation 2.36 was converted to a more compact notation $|\psi_\beta(\beta_0 \overrightarrow{k_0})\rangle \rightarrow \psi_\beta(\vec{r})$, and the channel potentials were included by following the procedure as below [74].

$$U'_\beta = V_\beta + iW_\beta \qquad 2.38$$

The imaginary part W_β accounts for the flux in channel β that is lost to other channels not included in the coupled channel equations. The non-Hermitian nature of H leads to a breakdown of the continuity equation. In cases where the channel coupling interaction U''_β is Hermitian, the continuity equation can be expressed using the relation provided below [74].

$$\overrightarrow{\nabla}.\sum_\beta \overrightarrow{J_\beta} = \frac{2}{\hbar}\sum_\beta W_\beta(\overrightarrow{r})\left|\psi_\beta(\vec{r})\right|^2 \neq 0 \qquad 2.39$$

In this context, $\vec{J}_\beta$represents the probability of current density in channel β. By integrating the above equation over a large sphere with a radius greater than the interaction range and applying the definition of absorption cross-section σ_β as described below [75,76], we can obtain the desired result.

$$\sigma_\beta = \frac{k}{E}\sum_\beta \langle\psi_\beta|W_\beta|\psi_\beta\rangle \qquad 2.40$$

The absorptive potential can be completed as below [69,65].

$$W_\beta = W_\beta^D + W_\beta^F \qquad 2.41$$

The flux lost to other direct reaction channels is accounted for by W_β^D, while W_β^F is used to account for fusion absorption. The cross-section of the fusion reaction can be expressed as follows, using the equations provided below [75, 77]:

$$\sigma_\beta = \frac{k}{E}\sum_\beta \langle \psi_\beta | W_\beta^F | \psi_\beta \rangle \qquad 2.42$$

Coupling among multiple channels can lead to an increase in the number of hard impacts in fusion interactions.

2.4 Fusion Barrier Distribution

Nuclear fusion occurs when waves transmit through a potential barrier and nuclear attraction overcomes Coulomb repulsion. The fusion barrier depends on the way the collision is described. Calculations of coupled channels involve static barriers that correspond to the frozen densities of the target and projectile. One of the most significant consequences of this approach is the enhancement of the total fusion reaction cross-section, σ_{fus}, at energies close to the Coulomb barrier V_b, with several orders of magnitude observed in various cases. The impact of coupling channels can be described by dividing the fusion barrier into multiple orders, which is known as the distribution of fusion barrier, D_{fus}, and can be obtained using the equations provided below [73, 78].

$$D_{fus}(E) = \frac{d^2F(E)}{dE^2} \qquad 2.43$$

The function denoted as F(E) represents the distribution of fusion barriers and is defined as follows:[78]

$$\mathrm{F(E)} = \mathrm{E}\sigma_{\mathrm{fus}}(\mathrm{E}) \qquad 2.44$$

The experimental determination of the distribution of fusion reaction barrier has been crucial in improving our understanding of fusion reactions. As previously mentioned, the distribution of fusion barrier provides information about the coupling channels involved in the collision. However, it is important to note that, as per equation 2.43, the distribution must be obtained from the values of the total fusion reaction cross-section, which are subject to both experimental and numerical uncertainties. Typically, the second derivative appearing in equation 2.43 is estimated using a three-point difference method, as described below [79, 80].

$$D_{fus}(E) \cong \frac{\mathrm{F(E+\Delta E)+F(E-\Delta E)-2F(E)}}{\mathrm{\Delta E^2}} \qquad 2.45$$

In this case, the cross-sectional data were measured at various excitation energy points, with an interval of ΔE. To determine the statistical error, the relation [79, 80] was utilized.

$$\delta D_{fus}^{stat}\ (\mathrm{E}) \approx \frac{[\ \ [\delta \mathrm{F(E+\Delta E)}]2+[\delta \mathrm{F(E-\Delta E)}]2+4[\delta \mathrm{FE}]2\ \ \ ]^{\frac{1}{2}}}{\mathrm{\Delta E^2}} \qquad 2.46$$

The uncertainty in the product of ($E\sigma_f$) for each collision energy, denoted by δF(E), is given as [79].

$$\delta D_{fus}^{stat}\ (\mathrm{E}) \cong \frac{\sqrt{6}\delta \mathrm{F}(E)}{[\Delta \mathrm{E}]^2} \qquad 2.47$$

Chapter Three

Results, Discussion and Conclusion

3.1 Introduction

The phenomenon of couple channels is widespread in nature and plays a critical part in nuclear reactions occurring at energies near the Coulomb barrier [81]. Numerous researchers have studied the impact of channel coupling on fusion reactions, and their findings suggest that coupling leads to a significant enhancement in the merger cross-section at sub-barrier energies during the collision of nuclei [82,83,84]. To describe the effect of breakup on fusion, the most appropriate theoretical approach is "the continuum discretized coupled-channel (CDCC) method". However, this technique falls short of giving an adequate depiction of some weakly correlated nucleus collisions, but it is an excellent model in most cases. Nevertheless, it is not feasible to account for the bound and continuum states of the projectile at the same time as nucleon transfer or inelastic channels in the target. As a result, many studies compare fusion data with calculations that disregard the effects of breakup and transfer channels. Any differences between the theoretical cross-sections and data are then attributed to processes such as breakup and transfer, which were not included in the calculations. In general, couple channel calculations are utilized to investigate fusion reactions theoretically [85].

Has been expanded "The continuum discretized coupled-channel (CDCC) method" procedure to investigate the effect of coupling between the elastic channel and the breakup channel by calculating the values of the cross-section, total fusion σ_{fus}, fusion barrier distribution D_{fus}, and fusion probability P_{fus} and comparing these values with the measured experimental data of the selected systems, which include tightly bound nuclei and involve the probability of transfer of one proton or one neutron.

3.2 Results and Discussion:

In this chapter, the calculations are performed by using two approaches, the quantum mechanics approach and the semi-classical approach using (CC code) and (SCF code) respectively for the two approaches, Table 3.1 shows "the Woods-Saxon parameters for the Akyüz-Winther potentials" that were used in the approaches: V_0, r_0, a_0, V_b, r_i W_0, a_i, L_{min}, and L_{max} with a coulomb barrier height V_b.

The distribution of the fusion barrier is determined using the three-point difference method, which is described in Appendix A.1 and A.2. Where we will review our results obtained using the quantum mechanical approaches and the semi-classical approach, for a group of selected systems $^{28}Si+^{90}Zr$, $^{28}Si+^{92}Zr$, $^{28}Si+^{94}Zr$, $^{28}Si+^{96}Zr$, $^{32}S+^{90}Zr$, $^{32}S+^{96}Zr$, $^{35}Cl+^{92}Zr$, $^{41}K+^{28}Si$, $^{45}K+^{28}Si$, $^{44}Ar+^{28}Si$, $^{41}K+^{16}O$ that include the probability of transferring one proton or one neutron to investigate the effect of coupling between the elastic channel and the breakup channel on the cross-section calculations Total fusion σ_{fus}, fusion barrier distribution D_{fus} and fusion probability P_{fus}.

For all figures in this chapter, the blue curves correspond to the quantum mechanical calculations with coupling and no-coupling, respectively. The blue curve with the spaces shows the results obtained with no-coupling. Similarly, the red curves, correspond to the semi-classical calculations with and no-coupling, respectively. The dashed red curve shows the results obtained no-coupling. The system's data regarding the position of the Coulomb sub-barrier V_b are sourced from the black arrow. The solid green balls represent experimental data.

Table 3.1: The Coulomb barrier height V_b and The Akyüz-Winther potential parameters.

Reactions	V_0(MeV)	r_0(fm)	a_0(fm)	W_0(MeV)	r_i(fm)	a_i(fm)	L_{max}	L_{min}	V_b(MeV)
$^{28}Si+^{90}Zr$	-146.1	1.055	0.800	-27.7	1.007	0.736	63	0	73.66
$^{28}Si+^{92}Zr$	-60.10	1.210	0.850	-14.4	1.007	0.736	31	0	72.15
$^{28}Si+^{94}Zr$	-140.0	1.100	0.800	-27.0	1.008	0.735	57	0	71.44
$^{28}Si+^{96}Zr$	-161.0	1.100	0.700	-28.3	1.008	0.735	61	0	70.80
$^{32}S+^{90}Zr$	-100.9	1.240	0.600	-39.3	1.018	0.729	142	0	82.28
$^{32}S+^{96}Zr$	-101.0	1.240	0.600	-34.3	1.020	0.728	83	0	81.25
$^{35}Cl+^{92}Zr$	-170.9	1.140	0.700	-40.6	1.027	0.724	86	0	82.88
$^{41}K+^{28}Si$	-46.00	1.212	0.655	-15.3	0.983	0.750	46	0	37.48
$^{45}K+^{28}Si$	-46.90	1.198	0.705	-15.6	0.986	0.748	45	0	36.86
$^{44}Ar+^{28}Si$	-72.90	1.180	0.602	-24.3	0.986	0.749	68	0	34.90
$^{41}K+^{16}O$	-72.20	1.070	0.750	-24.4	0.958	0.765	37	0	22.64

3.2.1 (^{28}Si+^{90}Zr) reaction :

Figure 1 depicts the theoretical and experimental σ_{fus}, D_{fus} and P_{fus} for the system ^{28}Si+^{90}Zr, obtained through a combination of quantum mechanical calculations and semi-classical methods. The semi-classical calculations, no-coupling, and coupling have a great concurrence with experimental data after exceeding V_b, and for below V_b, there is no concurrence with experimental data. For no-coupling and coupling quantum mechanical calculations, after exceeding V_b there is a special concurrence.

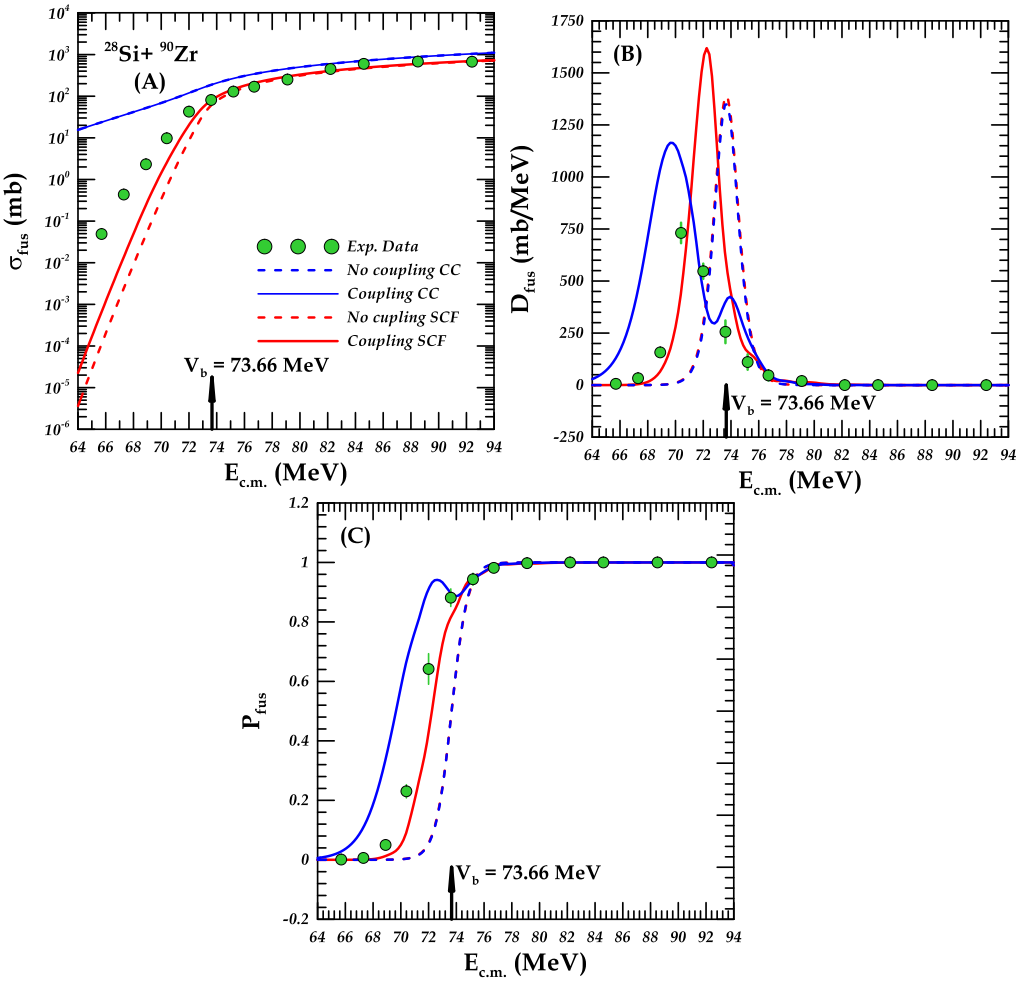

Figure 3.1: Displays the results of quantum mechanical and semi-classical calculations for the σ_{fus} (A), D_{fus} (B), and P_{fus} (C), alongside experimental data [86] for the system ^{28}Si+^{90}Zr.

3.2.2 (^{28}Si+^{92}Zr) reaction :

The calculation of σ_{fus}, D_{fus} and P_{fus} for the system ^{28}Si+^{92}Zr is shown in Fig.2. The calculations of the quantum mechanical and semi-classical methods is shown for both non-coupling and coupling. The semi-classical calculations, no-coupling, and coupling have a special concurrence with experimental data after exceeding V_b and below V_b. For no-coupling and coupling quantum mechanical calculations, after exceeding V_b there is a special concurrence.

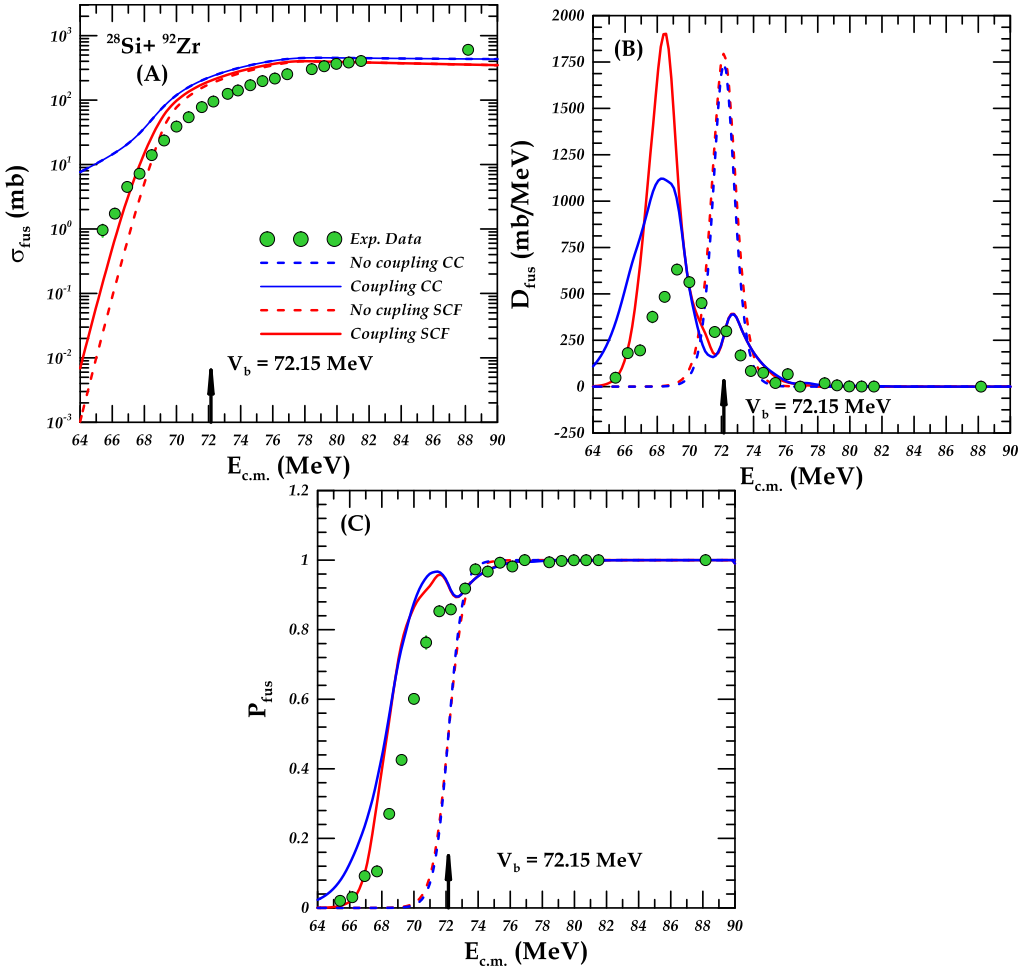

Figure 3.2: Displays the results of quantum mechanical and semi-classical calculations for the σ_{fus} (A), D_{fus} (B), and P_{fus} (C), alongside experimental data [87] for the system ^{28}Si+^{92}Zr.

3.2.3 (^{28}Si+^{94}Zr) reaction :

Figure 2 depicts the computation of σ_{fus}, D_{fus} and P for the system ^{28}Si+^{94}Zr. The computations of the quantum mechanical and semi-classical approaches for non-coupling and coupling are shown. The data used in this study are taken from Ref. [88]. The semi-classical calculations, no-coupling, and coupling have a good concurrence with experimental data after exceeding V_b, and for below V_b, there is a special concurrence. For no-coupling and coupling quantum mechanical calculations, there is no concurrence.

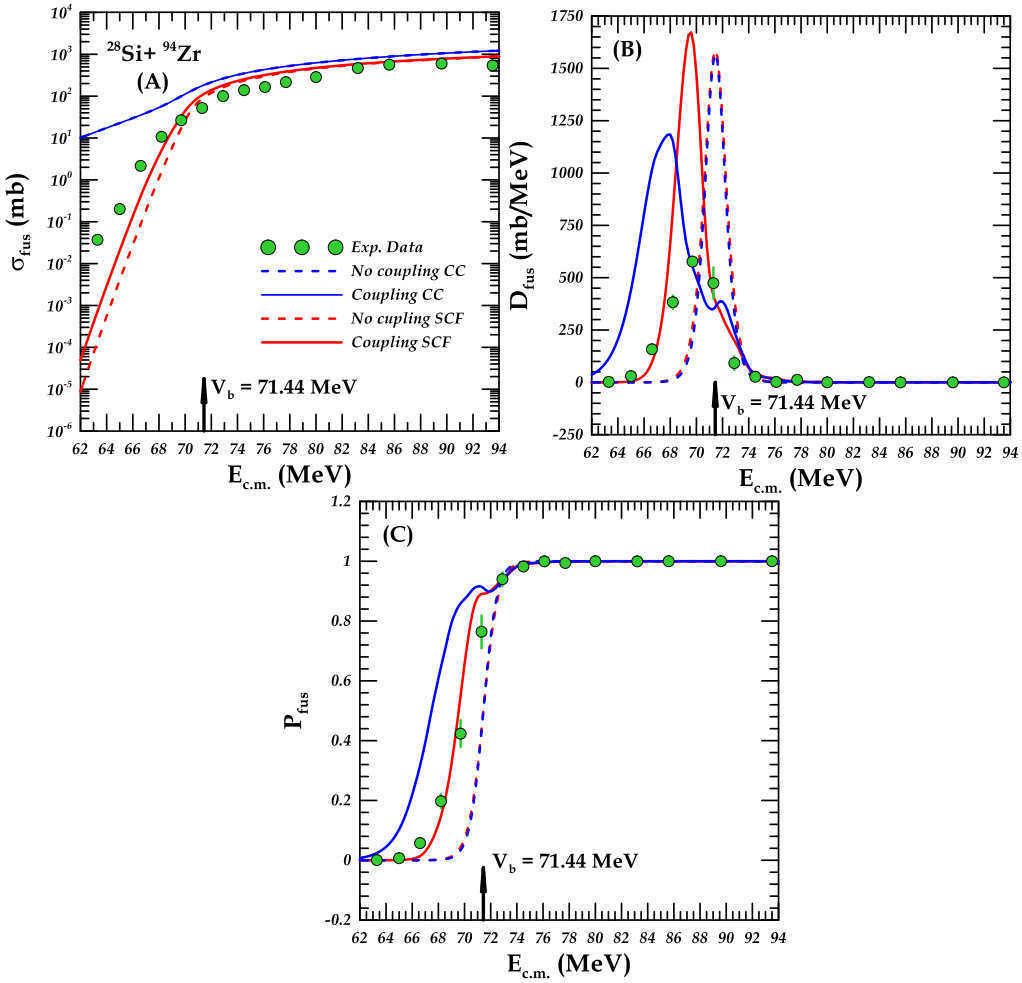

Figure 3.3: Displays the results of quantum mechanical and semi-classical calculations for the σ_{fus} (A), D_{fus} (B), and P_{fus} (C), alongside experimental data [86] for the system ^{28}Si+^{94}Zr.

3.2.4 (^{28}Si+^{96}Zr) system :

The theoretical and experimental σ_{fus}, D_{fus}, and P_{fus} for the system ^{28}Si+^{96}Zr are shown in Fig.4. Above V_b: the semi-classical computations without coupling and coupling show excellent agreement with the experimental data, whereas, for quantum mechanical calculation, there is good agreement with the data. below V_b: below Coulomb's barrier, results improved in couple channel calculation for semi-classical approaches, for quantum mechanical calculations the results of couple channel calculation and without coupling exaggerated the results.

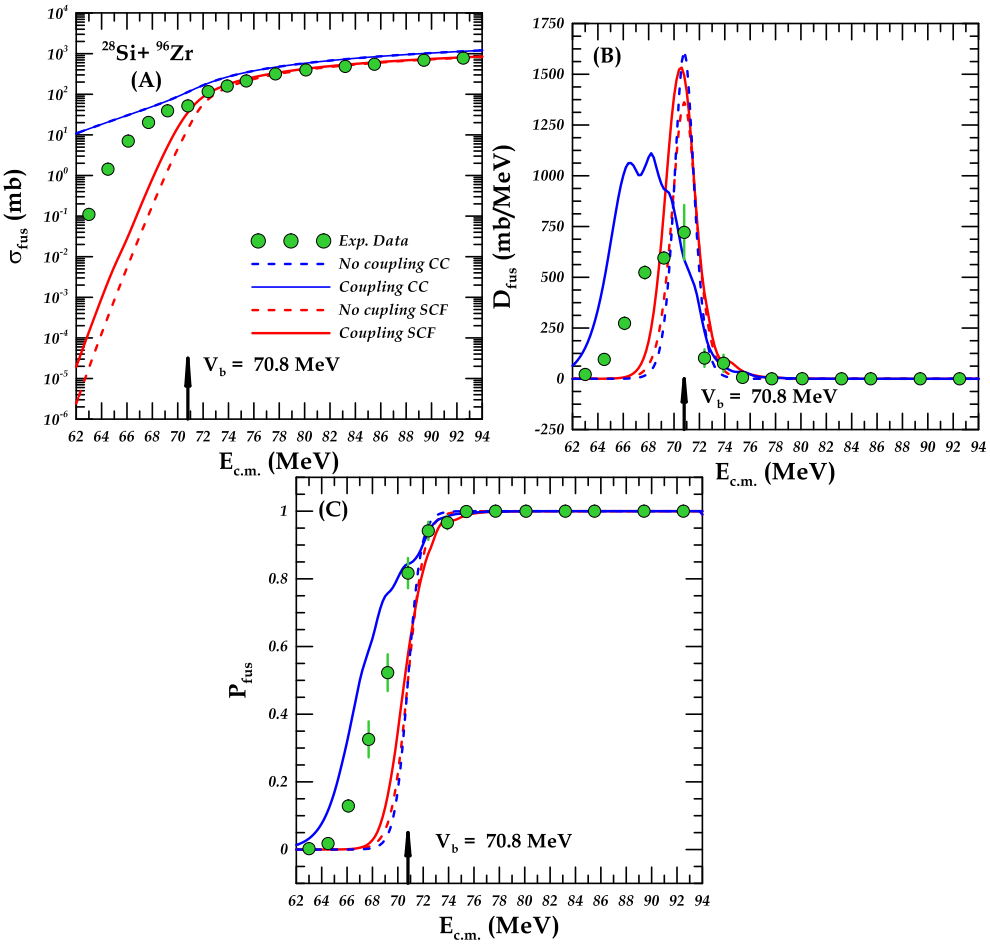

Figure 3.4: Displays the results of quantum mechanical and semi-classical calculations for the σ_{fus} (A), D_{fus} (B), and P_{fus} (C), alongside experimental data [89] for the system ^{28}Si+^{96}Zr**.**

3.2.5 (^{32}S+^{90}Zr) system :

The theoretical and experimental σ_{fus}, D_{fus}, and P_{fus} for the system ^{32}S+^{90}Zr are shown in Fig.5. Above V_b: the semi-classical computations with no coupling and coupling show very good agreement with the experimental data, whereas, for quantum mechanical calculation, there is good agreement Behavioral aspect, but it is more exaggerated than the available experimental data. below V_b: the results improved in couple channel calculation for semi-classical approaches, for quantum mechanical calculations it exaggerated the results

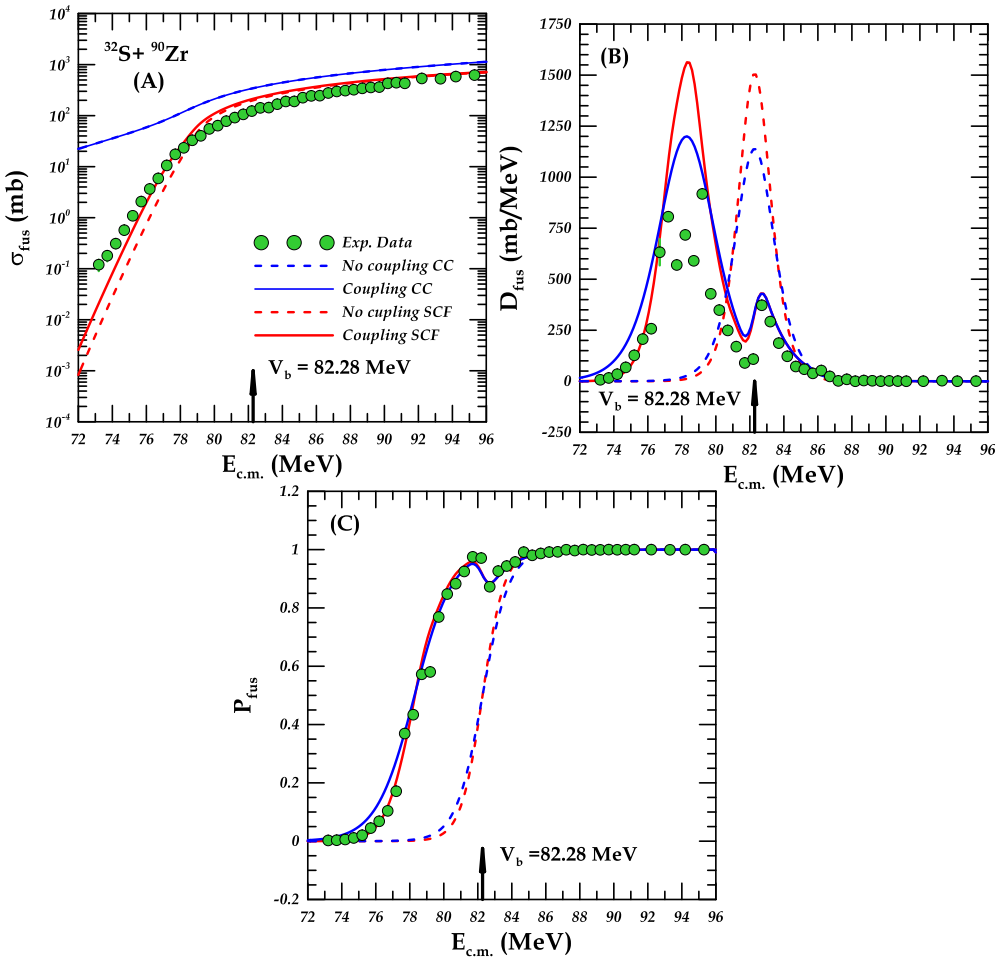

Figure 3.5: Displays the results of quantum mechanical and semi-classical calculations for the σ_{fus} (A), D_{fus} (B), and P_{fus} (C), alongside experimental data [89] for the system ^{32}S+^{90}Zr**.**

3.2.6 (^{32}S+^{96}Zr) system :

The theoretical and experimental σ_{fus}, D_{fus}, and P_{fus} for the system ^{32}S+^{96}Zr are shown in Fig.6. Above V_b: the semi-classical computations with no coupling and coupling show excellent agreement with the experimental data, whereas, for quantum mechanical calculation, there is good agreement Behavioral aspect, but it is more exaggerated than the available experimental data. below V_b: the results improved in couple channel calculation for semi-classical approaches, for quantum mechanical calculations the results of couple channel calculation and without coupling exaggerated the results.

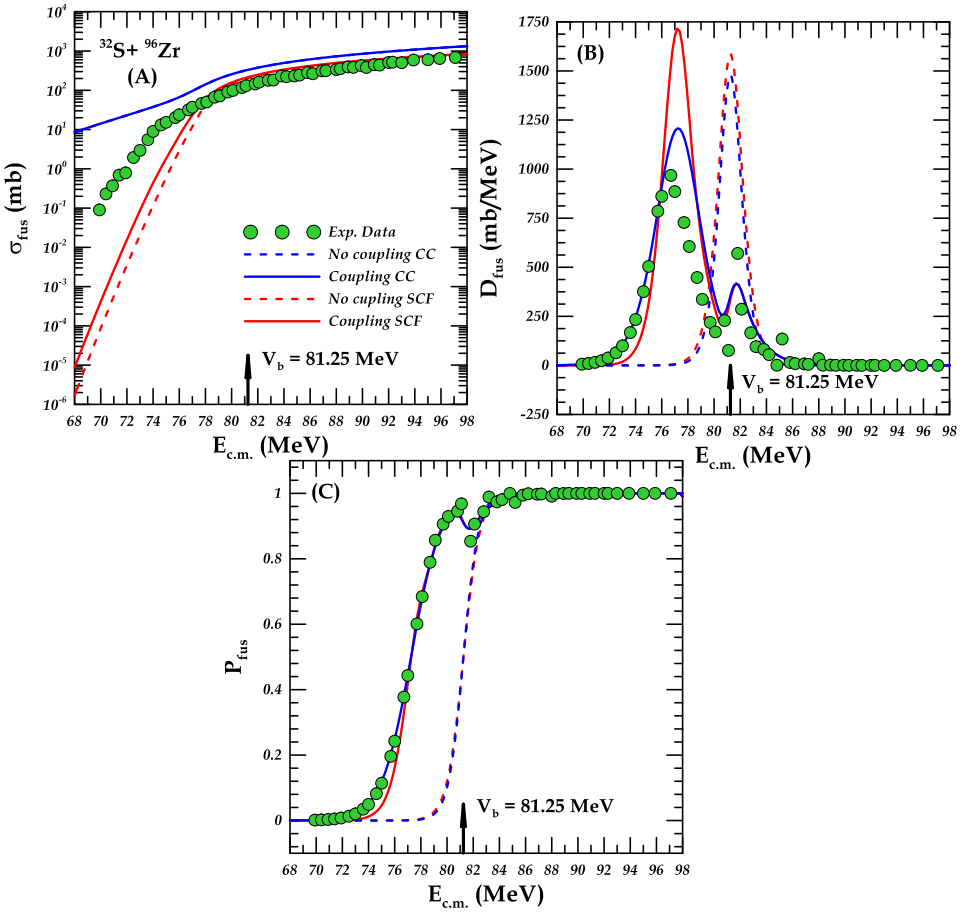

Figure 3.6: Displays the results of quantum mechanical and semi-classical calculations for the σ_{fus} (A), D_{fus} (B), and P_{fus} (C), alongside experimental data [90] for the system ^{32}S+^{96}Zr.

3.2.7 (^{35}Cl+^{92}Zr) system :

The theoretical and experimental σ_{fus}, D_{fus}, and P_{fus} for the system ^{35}Ci+^{92}Zr are shown in Fig.7. Above V_b: the semi-classical computations with no coupling and coupling show excellent agreement with the experimental data, whereas, for quantum mechanical calculation, there is good agreement Behavioral aspect, but it is more exaggerated than the available experimental data. below V_b: the results improved in couple channel calculation for semi-classical approaches, for quantum mechanical calculations the results of couple channel calculation and without coupling were very exaggerated the results.

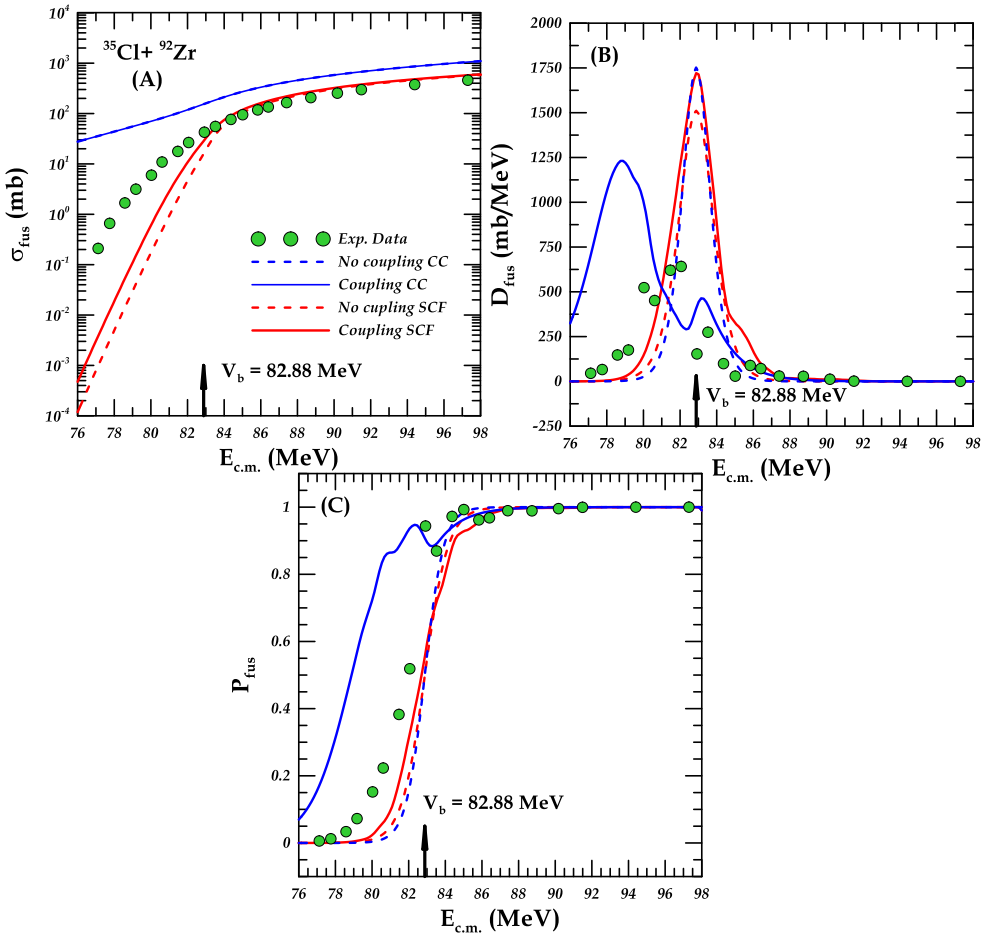

Figure 3.7: Displays the results of quantum mechanical and semi-classical calculations for the σ_{fus} (A), D_{fus} (B), and P_{fus} (C), alongside experimental data [87] for the system ^{35}Cl+^{92}Zr**.**

3.2.8 (^{41}K+ ^{28}Si) reaction :

The theoretical and experimental σ_{fus}, D_{fus} and P_{fus} for the system ^{41}K+^{28}Si are shown in Fig.8, and are obtained through the calculations of the quantum mechanical calculations and semi-classical methods. The semi-classical calculations, no-coupling have a special concurrence with experimental data after exceeding V_b, and for below V_b there is no concurrence, and for coupling, there is a great concurrence. For quantum mechanical calculations, there is a great concurrence after exceeding V_b.

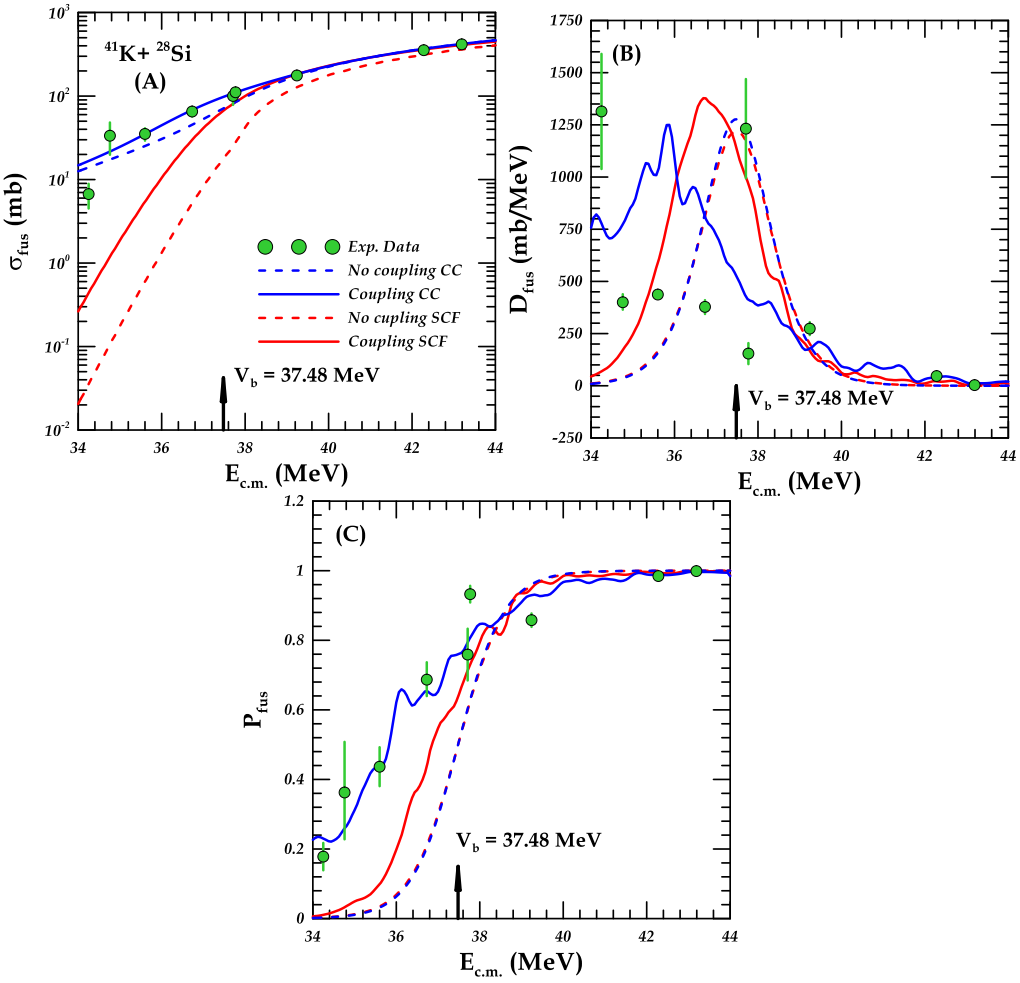

Figure 3.8: Displays the results of quantum mechanical and semi-classical calculations for the σ_{fus} (A), D_{fus} (B), and P_{fus} (C), alongside experimental data [88] for the system ^{41}K+^{28}Si**.**

3.2.9 (^{45}K+ ^{28}Si) reaction :

Fig.9 depicts the theoretical and experimental σ_{fus}, D_{fus} and P_{fus} for the system ^{45}K+^{28}Si, and are obtained through a combination of quantum mechanical calculations and semi-classical methods. The semi-classical calculations, no-coupling, and coupling have a good concurrence with experimental data after exceeding V_b. For no-coupling and coupling quantum mechanical calculations, below V_b there is a great concurrence.

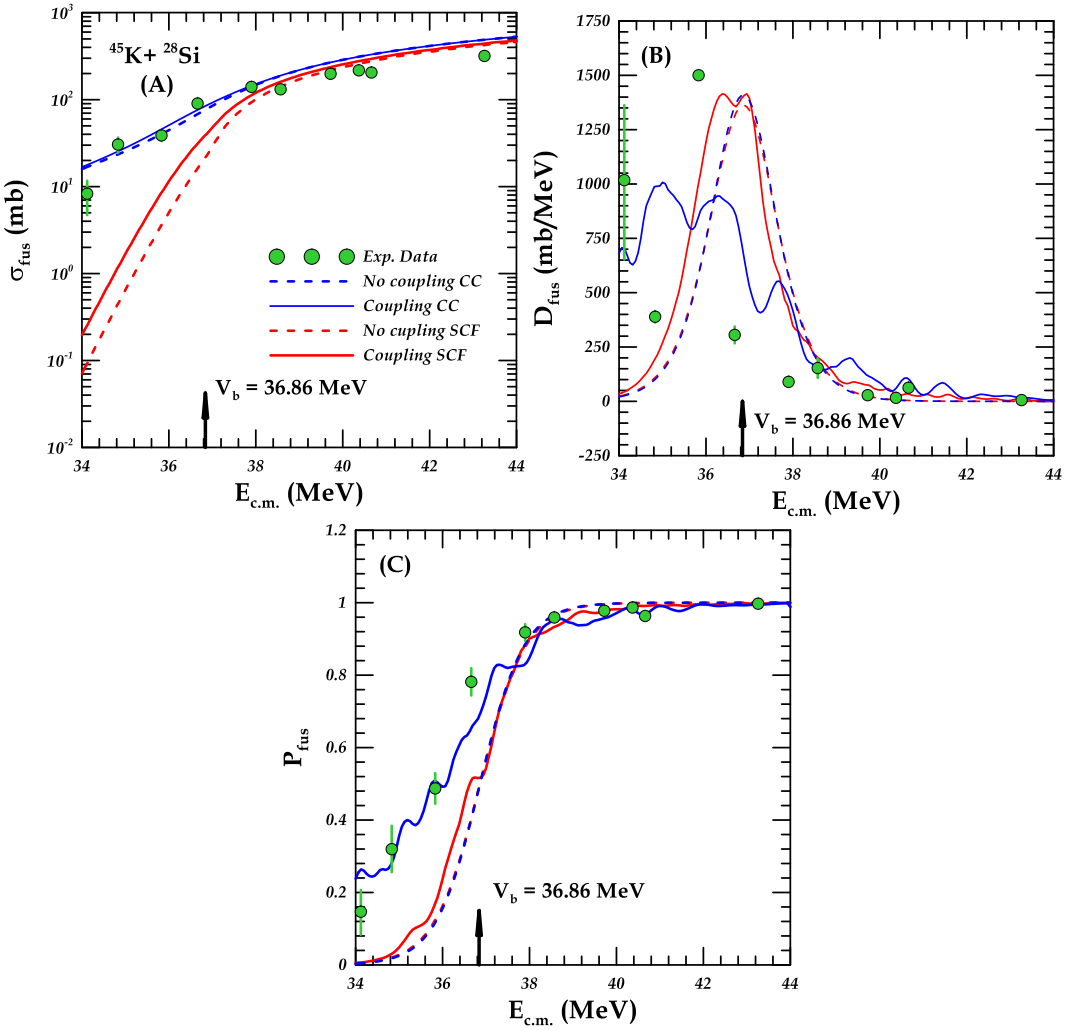

Figure 3.9: Displays the results of quantum mechanical and semi-classical calculations for the σ_{fus} (A), D_{fus} (B), and P_{fus} (C), alongside experimental data [88] for the system ^{45}K+^{28}Si.

3.2.10 (^{44}Ar+ ^{28}Si) reaction :

Fig.10 depicts the theoretical and experimental σ_{fus}, D_{fus} and P_{fus} for the system ^{44}Ar+^{28}Si, and are obtained through a combination of quantum mechanical calculations and semi-classical methods. The semi-classical calculations, no-coupling, and coupling have a good Behavioral aspect with experimental data and special concurrence. For no-coupling and coupling quantum mechanical calculations, below and above V_b there is no concurrence.

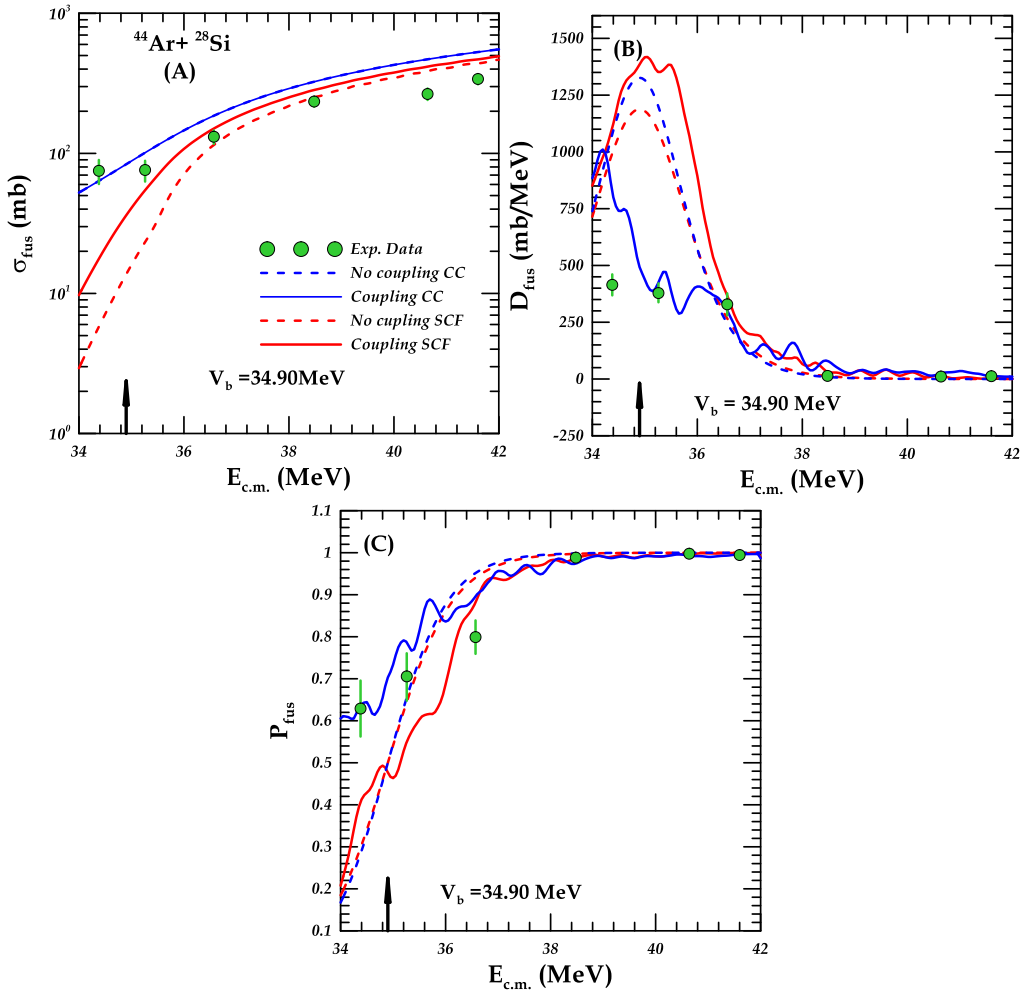

Figure 3.10: Displays the results of quantum mechanical and semi-classical calculations for the σ_{fus} (A), D_{fus} (B), and P_{fus} (C), alongside experimental data [88] for the system ^{44}Ar+^{28}Si.

3.2.11 (^{41}K+ ^{16}O) reaction :

Fig.11 depicts the theoretical and experimental σ_{fus}, D_{fus} and P_{fus} for the system ^{41}K+^{16}O, and are obtained through a combination of quantum mechanical calculations and semi-classical methods. The semi-classical calculations, for the no-coupling, have a good concurrence with experimental data. For no-coupling and coupling quantum mechanical calculations, there is no concurrence.

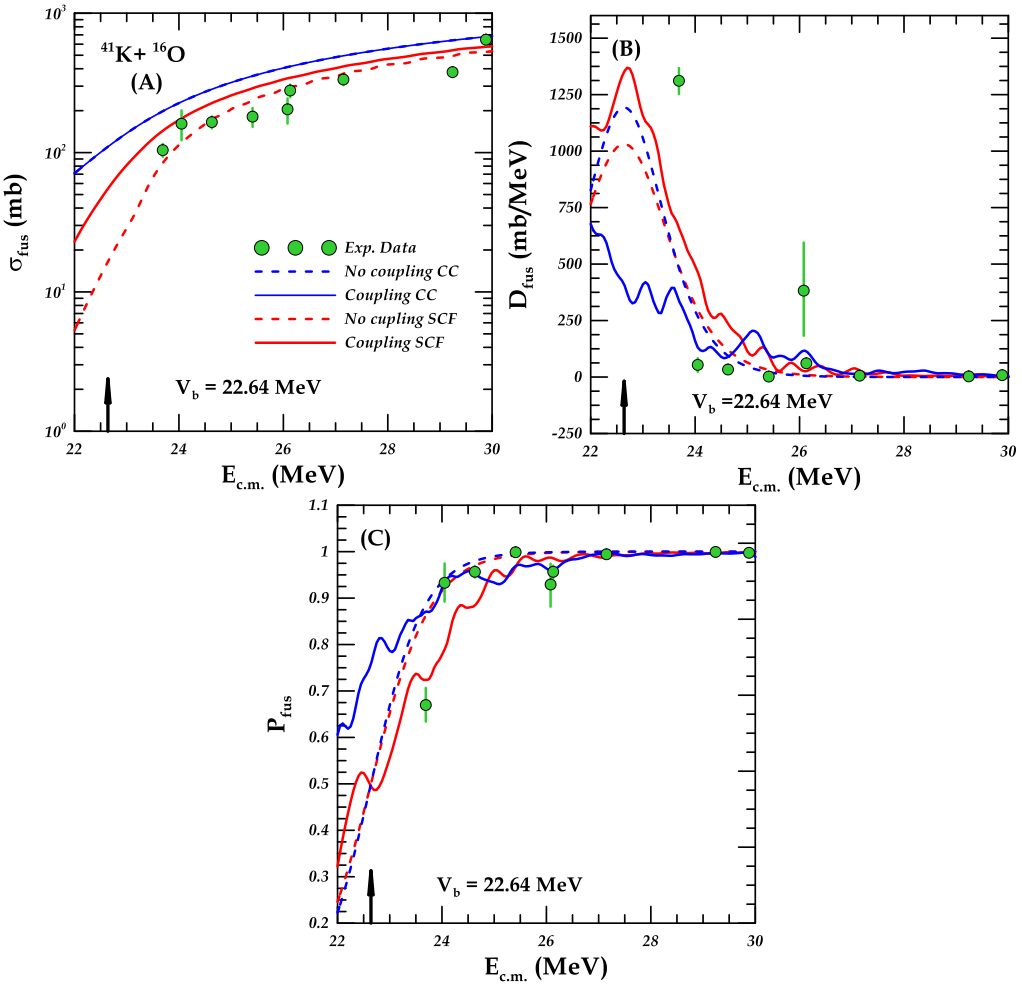

Figure 3.11: Displays the results of quantum mechanical and semi-classical calculations for the σ_{fus} (A), D_{fus} (B), and P_{fus} (C), alongside experimental data [88] for the system ^{41}K+^{16}O.

3.3 conclusion:

The conclusions derived from this study highlight the importance of including the following key points as integral findings:

1. The semi-classical calculations succeeded in describing experimental data in most of the studied systems above Coulomb barrier V_b.

2. The quantum mechanical calculations and semi-classical calculations have a shortfall in describing the experimental data for most of the studied systems below the Coulomb barrier V_b.

3. Adding the effect of coupling between the elastic and the breakup channels is found to be very essential that improving the fusion cross-section calculations below the Coulomb barrier V_b.

4. When the coupling instrument was included in the calculations of the semi-classical and quantum mechanics approaches, it was found to have a clear effect on the calculations of D_{fus} and P_{fus} where the results improved below V_b. The reason for this improvement is that the coupling effects are more significant at lower energies, leading to a more complex interaction between the elastic channels and the breakup channels. Introducing coupling conditions into the calculations takes into account the exchange of flow between these channels, and the slight overestimation of the results above V_b can be attributed to the fact that the fusion process becomes more controlled by the elastic channel at higher energies, and the coupling effects become less significant.

6. The stripping of the neutron or proton or its pickup by the interacting nuclei before the nuclear fusion process occurs improves the nuclear structure of the colliding nuclei, and this leads to improving the dynamics of the interaction, the coupling between the elastic channel and the breakup channel is more effective.

3.4 The Future Works

1. Using other models to perform the calculations and compare them with the extracted results to verify and compare the results, for example, the Optical Model and the Yakawa potential.

2. Developing the CC code and adding multi-channels that may improve the results, especially below the Coulomb barrier V_b, such as adding the effects of deformation nuclei to the calculations.

3. Studying systems in which the projectile and target nuclei contain an unpaired neutron or proton, to achieve a greater understanding of this effect on calculations.

Reference

[1] J.X. Wei, "Barrier distributions in heavy ion induced fusion reactions," Nucl. Phys. A, vol. 557, no. 3-4, pp. 645-657, 1993.

[2] D.L. Hill and J.A. Wheeler, "Nuclear constitution and the interpretation of fission phenomena," Physical Review, vol. 89, no. 5, p. 1102, 1953.

[3] R.G. Stokstad, Y. Eisen, S. Kaplanis, D. Pelte, U. Smilansky, and I. Tserruya, "Effect of nuclear deformation on heavy-ion fusion," Physical Review Letters, vol. 41, no. 7, p. 465, 1978.

[4] R.G. Stokstad, Y. Eisen, S. Kaplanis, D. Pelte, U. Smilansky, and I. Tserruya, "Fusion of O16+Sm148,150,152,154 at sub-barrier energies," Physical Review C, vol. 21, no. 6, p. 2427, 1980.

[5] M. Beckerman, M. Salomaa, A. Sperduto, H. Enge, J. Ball, A. DiRienzo, S. Gazes, Y. Chen, J.D. Molitoris, and M. Nai-Feng, "Dynamic influence of valence neutrons upon the complete fusion of massive nuclei," Physical Review Letters, vol. 45, no. 18, p. 1472, 1980.

[6] W. Reisdorf, F.P. Hessberger, K.D. Hildenbrand, S. Hofmann, G. Münzenberg, K.H. Schmidt, J.H.R. Schneider, W.F.W. Schneider, K. Sümmerer, G. Wirth, and J.V. Kratz, "Influence of collective surface motion on the threshold behavior of nuclear fusion," Physical Review Letters, vol. 49, no. 25, p. 1811, 1982.

[7] M. Beckerman, "Experimental overview of sub-barrier fusion," Nuclear Physics A, vol. 452, no. 1, pp. 97-114, 1986.

[8] L.C. Vaz and J.M. Alexander, "Systematics of reaction cross sections and interaction barriers for charged particles," Physical Review C, vol. 10, no. 2, p. 464, 1974.

[9] W. Reisdorf, F.P. Hessberger, K.D. Hildenbrand, S. Hofmann, G. Münzenberg, K.H. Schmidt, J.H.R. Schneider, W.F.W. Schneider, K.

Sümmerer, G. Wirth, and J.V. Kratz, "Fusion near the threshold: A comparative study of the systems 40Ar+112,116,122sn and 40Ar+144,148,154Sm," Nuclear Physics A, vol. 438, no. 1, pp. 212-252, 1985.

[10] P.H. Stelson, "Neutron flow between nuclei as the principal enhancement mechanism in heavy-ion subbarrier fusion," Physics Letters B, vol. 205, no. 2-3, pp. 190-194, 1988.

[11] N. Jain, S. Rana, J.T. Majekodunmi, R. Kumar, and M. Bhuyan, "Effect of Shapes Degrees of Freedom on the Fusion Cross-Sections of 16O+154Sm and 18O+148Nd," ECS Transactions, vol. 107, no. 1, p. 12723, 2022.

[12] K. Hagino, "Sub-barrier fusion reactions," arXiv preprint arXiv:2201.08061, 2022.

[13] K.P. Santhosh and V.B. Jose, "Heavy-ion fusion reactions of 16o on spherical/deformed 144-154Smtargets using coulomb and proximity potentials," Romanian Reports in Phys, vol. 66, no. 4, pp. 939-951, 2014.

[14] N. Chauhan and S.S. Godre, "Coupled-channel calculation of fusion cross section of 16O+154Sm reaction using modified Proximity Potential," in Proceedings of the DAE Symp. on Nucl. Phys, vol. 65, p. 243, 2021.

[15] R. Pengo, D. Evers, K.E.G. Löbner, U. Quade, K. Rudolph, S.J. Skorka, and I. Weidl, "Nuclear structure effects in sub-barrier fusion cross sections," Nuclear Physics A, vol. 411, no. 2, pp. 255-274, 1983.

[16] P.R.S. Gomes, J. Lubian, I. Padron, R.M. Anjos, D.R. Otomar, L.C. Chamon, and E. Crema, "Fusion, break-up and scattering of weakly bound nuclei," Revista mexicana de física, vol. 52, pp. 23-29, 2006.

[17] P.R.S. Gomes, I. Padron, E. Crema, O.A. Capurro, J.F. Niello, A. Arazi, G.V. Martí, J. Lubian, M. Trotta, A.J. Pacheco, and J.E. Testoni,

"Comprehensive study of reaction mechanisms for the Be9+Sm144 system at near-and sub-barrier energies," Physical Review C, vol. 73, no. 6, p. 064606, 2006.

[18] G.D. Kolinger, L.F. Canto, R. Donangelo, and S.R. Souza, "Semiclassical calculations of complete and incomplete fusion in collisions of weakly bound nuclei," Physical Review C, vol. 98, no. 4, p. 044604, 2018.

[19] L.F. Canto, P.R.S. Gomes, R. Donangelo, J. Lubian, and M.S. Hussein, "Recent developments in fusion and direct reactions with weakly bound nuclei," Physics Reports, vol. 596, pp. 1-86, 2015.

[20] M. Prasanna, V.V. Parkar, V. Jha, A. Parmar, B.A. Kanagalekar, and B.G. Hegde, "Role of neutron transfer in the reaction mechanism of 9Be+169Tm, 181Ta, 187Re and 197Au systems," Nuclear Physics A, vol. 1029, p. 122570, 2023.

[21] N.K. Deb, K. Kalita, H. Al Rashid, S. Nath, J. Gehlot, N. Madhavan, R. Biswas, R.N. Sahoo, P.K. Giri, A. Das and T. Rajbongshi, "Role of neutron transfer in the sub-barrier fusion cross section in O18+Sn116," Physical Review C, vol. 102, no. 3, p. 034603, Sep. 2020.

[22] Y.E. Penionzhkevich, R.A. Astabatyan, N.A. Demekhina, G.G. Gulbekian, R. Kalpakchieva, A.A. Kulko, S.M. Lukyanov, E.R. Markaryan, V.A. Maslov, Y.A. Muzychka and Y.T. Oganessian, "Excitation functions of fusion reactions and neutron transfer in the interaction of 6He with 197Au and 206Pb," The European Physical Journal A, vol. 31, pp. 185-194, Jan. 2007.

[23] H.A. Bethe, "Energy production in stars," Physical Review, vol. 55, no. 5, p. 434, Mar. 1939.

[24] G. Gamow, "The origin of elements and the separation of galaxies," Physical Review, vol. 74, no. 4, p. 505, Aug. 1948.

[25] G. Gamow, "The evolution of the universe," Nature, vol. 162, no. 4122, pp. 680-682, Oct. 1948.

[26] C. Guillemaut, "Modelling of the edge of a fusion plasma towards ITER and experimental validation on JET," Univ. Aix-Marseille, no. FRCEA-TH--5836. 2013

[27] M.D. Mathew, "Nuclear energy: A pathway towards mitigation of global warming," Progress in Nuclear Energy, vol. 143, p. 104080, Sep. 2022.

[28] L.F. Canto, P.R.S. Gomes, J. Lubian, L.C. Chamon and E. Crema, "Disentangling static and dynamic effects of low breakup threshold in fusion reactions," Journal of Physics G: Nuclear and Particle Physics, vol. 36, no. 1, p. 015109, Jan. 2008.

[29] B. Wang, W.J. Zhao, P.R.S. Gomes, E.G. Zhao and S.G. Zhou, "Systematic study of breakup effects on complete fusion at energies above the Coulomb barrier," Physical Review C, vol. 90, no. 3, p. 034612, Sep. 2014.

[30] K.J. Cook, "Zeptosecond Dynamics of Transfer-Triggered Breakup: Mechanisms, Timescales, and Consequences for Fusion," Springer, 2018.

[31] A. Diaz-Torres, "Modelling incomplete fusion dynamics of weakly bound nuclei at near-barrier energies," Journal of Physics G: Nuclear and Particle Physics, vol. 37, no. 7, p. 075109, Jul. 2010.

[32] P.R.S. Gomes, I. Padron, E. Crema, O.A. Capurro, J.F. Niello, A. Arazi, G.V. Martí, J. Lubian, M. Trotta, A.J. Pacheco and J.E. Testoni, "Comprehensive study of reaction mechanisms for the Be9+Sm144 system at near-and sub-barrier energies," Physical Review C, vol. 73, no. 6, p. 064606, Jun. 2006.

[33] M. Beckerman, M. Salomaa, A. Sperduto, H. Enge, J. Ball, A. DiRienzo, S. Gazes, Y. Chen, J.D. Molitoris and M. Nai-Feng, "Dynamic influence

of valence neutrons upon the complete fusion of massive nuclei," Physical Review Letters, vol. 45, no. 18, p. 1472, Oct. 1980.

[34] R.A. Broglia, C.H. Dasso, S. Landowne and A. Winther, "Possible effect of transfer reactions on heavy ion fusion at sub-barrier energies," Physical Review C, vol. 27, no. 5, p. 2433, May 1983.

[35] N. Rowley, I.J. Thompson and M.A. Nagarajan, "Neutron flow and necking in heavy-ion fusion reactions," Physics Letters B, vol. 282, no. 3-4, pp. 276-280, Nov. 1992.

[36] H. Timmers, D. Ackermann, S. Beghini, L. Corradi, J.H. He, G. Montagnoli, F. Scarlassara, A.M. Stefanini and N. Rowley, "A case study of collectivity, transfer and fusion enhancement," Nuclear Physics A, vol. 633, no. 3, pp. 421-442, Oct. 1998.

[37] V.Y. Denisov, "Subbarrier heavy ion fusion enhanced by nucleon transfer," The European Physical Journal A-Hadrons and Nuclei, vol. 7, pp. 87-99, Jan. 2000.

[38] V.I. Zagrebaev, "Sub-barrier fusion enhancement due to neutron transfer," Physical Review C, vol. 67, no. 6, p. 061601, Jun. 2003.

[39] A. Bonaccorso, D.M. Brink and C.A. Bertulani, "Proton vs neutron halo breakup," Physical Review C, vol. 69, no. 2, p. 024615, Feb. 2004.

[40] C. Simenel, M. Bender, P. Chomaz, T. Duguet and G. De France, "Quantum calculation of Coulomb reorientation and near-barrier fusion," in AIP Conference Proceedings, vol. 853, no. 1, pp. 303-308, Aug. 2006.

[41] B. K. Nayak, R. K. Choudhury, A. Saxena, P. K. Sahu, R. G. Thomas, D. C. Biswas, B. V. John, E. T. Mirgule, Y. K. Gupta, M. Bhike, and H. G. Rajprakash, "Evidence for Coulomb effects on the fusion barrier distribution for deformed projectile nuclei," Physical Review C, vol. 75, no. 5, p. 054615, May 2007.

[42] V. V. Sargsyan, G. G. Adamian, N. V. Antonenko, W. Scheid, and H. Q. Zhang, "Effects of nuclear deformation and neutron transfer in capture processes, and fusion hindrance at deep sub-barrier energies," Physical Review C, vol. 84, no. 6, p. 064614, Dec. 2011.

[43] V. V. Sargsyan, G. G. Adamian, N. V. Antonenko, W. Scheid, and H. Q. Zhang, "Role of neutron transfer in capture processes at sub-barrier energies," Physical Review C, vol. 85, no. 2, p. 024616, Feb. 2012.

[44] G. L. Zhang, X. X. Liu, and C. J. Lin, "Systematic analysis of the effect of a positive Q-value neutron transfer in fusion reactions," Physical Review C, vol. 89, no. 5, p. 054602, May 2014.

[45] F. K. Ahmed, F. A. Majeed, and T. M. Abbass, "The Effect of Breakup on the Total Fusion Reaction Cross Section of Stable Weakly Bound Nuclei," University of Babylon, 2013.

[46] F. A. Majeed and Y. A. Abdul-Hussien, "Semiclassical treatment of fusion and breakup processes of 6, 8 He halo nuclei," Journal of Theoretical and Applied physics, vol. 10, no. 2, pp. 107-112, 2016.

[47] F. A. Majeed, R. S. Hamodi, and F. M. Hussian, "Effect of coupled channels on semiclassical and quantum mechanical calculations for heavy ion fusion reactions," Journal of Computational and Theoretical Nanoscience, vol. 14, no. 5, pp. 2242-2247, 2017.

[48] F. A. Majeed, K. H. AlAteah, and M. S. Mehemed, "Coupled channel calculations using semi-classical and quantum mechanical approaches for light and medium mass systems," International Journal of Nuclear Energy Science and Technology, vol. 11, no. 4, pp. 291-308, 2017.

[49] F. M. Hussain, F. A. Majeed, and Y. A. Abdul-Hussien, "Description of coupled-channel in Semiclassical treatment of heavy ion fusion reactions," in IOP Conference Series: Materials Science and Engineering, vol. 571, no. 1, p. 012113, Jul. 2019.

[50] F. M. Hussain, F. A. Majeed, and M. H. Meteab, "Investigation of the Calculation of Coupled Channels for Some Halo Systems," Ukrainian Journal of Physics, vol. 65, no. 11, pp. 951-951, 2020.

[51] M. S. Mehemed, S. M. Obaid, and F. A. Majeed, "Coupled channels calculation of fusion reaction for selected medium systems," International Journal of Nuclear Energy Science and Technology, vol. 14, no. 2, pp. 165-180, 2020.

[52] M. H. Abd Madhi and F. A. Majeed, "Fusion reaction study of halo system by quantum mechanical-based model for 6 He+ 64 Zn, 8 B+ 58 Ni and 8 He+ 197 Au systems," Bulletin of the Polish Academy of Sciences: Technical Sciences, vol. 69, no. 4, 2021.

[53] S. A. Abbas, A. A. Hussein, S. M. Obaid, and N. A. Mohammed, "Fusion Reaction Study of some Selected Halo Systems," Baghdad Science Journal, vol. 20, no. 2, pp. 0458-0458, 2023.

[54] W. Chen, D. Y. Pang, H. Guo, Y. Tao, W. Sun, and Y. Ying,"Continuum-discretized coupled-channels calculations for Li 6 fusion reactions with closed channels," Physical Review C, vol. 107, no. 6, p. 064610, Jun. 2023.

[55] C. H. Dasso, S. Landowne, and A. Winther, "Channel-coupling effects in heavy-ion fusion reactions," Nuclear Physics A, vol. 405, pp. 381-396, 1983.

[56] J. E. Johnstone, "The influence of shell structure on near-barrier fusion of neutron-rich nuclei" (PhD thesis), Department of Physics, Indiana University, 2022.

[57] G. Wentzel, "Eine verallgemeinerung der quantenbedingungen für die zwecke der wellenmechanik," Zeitschrift für Physik, vol. 38, no. 6-7, pp. 518-529, 1926.

[58] H. A. Kramers, "Wellenmechanik und halbzahlige Quantisierung," Zeitschrift für Physik, vol. 39, no. 10-11, pp. 828-840, 1926.

[59] L. Brillouin, "La mécanique ondulatoire de Schrödinger: une méthode générale de resolution par approximations successives," C. R. Hebd. Acad. Sci., vol. 183, pp. 24, 1926.

[60] H. Jeffreys, "On certain equations of the second order," Proceedings of the London Mathematical Society, vol. 23, no. 1, pp. 428, 1925.

[61] J. L. Dunham, "The Wentzel-Brillouin-Kramers method of solving the wave equation," Physical Review, vol. 41, no. 6, pp. 713-720, 1932.

[62] H. Feshbach, "A unified theory of nuclear reactions. II," Annals of Physics, vol. 19, no. 2, pp. 287-313, 1962.

[63] M. Abramowitz and I. A. Stegun, Handbook of Mathematical Functions. New York, NY: Dover Publications Inc., 1964.

[64] G. G. Stokes, "On the discontinuity of arbitrary constants that appear as multipliers of semi-convergent series," Acta Mathematica, vol. 26, no. 1, pp. 393-397, 1902.

[65] A. Safari, "Some recent developments in WKB approximation," M.Sc. Thesis, McMaster University, Hamilton, ON, Canada, 2013.

[66] K. Hagino, N. Takigawa, M. Dasgupta, D. J. Hinde, and J. R. Leigh, "Validity of the linear coupling approximation in heavy-ion fusion reactions at sub-barrier energies," Physical Review C, vol. 55, no. 1, pp. 276-280, 1997.

[67] A. M. Stefanini, D. Ackermann, L. Corradi, D. R. Napoli, C. Petrache, P. Spolaore, P. Bednarczyk, H. Q. Zhang, S. Beghini, G. Montagnoli, L. Mueller, F. Scarlassara, G. F. Segato, F. Sorame, and N. Rowley, "Influence of Complex Surface Vibrations on the Fusion of 58Ni + 64Ni," Physical Review Letters, vol. 74, no. 6, pp. 864-867, 1995.

[68] K. Hagino, N. Takigawa, A. B. Balantekin, and J. R. Bennett, "Path integral approach to no-Coriolis approximation in heavy-ion collisions," Physical Review C, vol. 52, no. 1, pp. 286-291, 1995.

[69] R. Lindsay and N. Rowley, "Approximate treatment of coupled-channels effects in sub-barrier fusion," Journal of Physics G: Nuclear Physics, vol. 10, no. 6, pp. 805-812, 1984.

[70] K. Hagino, N. Rowley, and A. T. Kruppa, "A program for coupled-channel calculations with all order couplings for heavy-ion fusion reactions," Computer Physics Communications, vol. 123, no. 1-3, pp. 143-152, 1999.

[71] D. J. Griffiths and D. F. Schroeter, Introduction to Quantum Mechanics, 3rd ed. Cambridge, UK: Cambridge University Press, 2018.

[72] S. Landowne and S. C. Pieper, "Coupled-channels fusion calculations for 58Ni + 58Ni," Physical Review C, vol. 29, no. 4, pp. 1352-1363, 1984.

[73] L. F. Canto, P. R. S. Gomes, R. Donangelo, and M. S. Hussein, "Fusion and breakup of weakly bound nuclei," Physics Reports, vol. 424, no. 1-2, pp. 1-111, 2006.

[74] N. Austern, Direct Nuclear Reaction Theory. New York, NY: Wiley, 1970.

[75] W. H. Z. Cardenas, L. F. Canto, R. Donangelo, M. S. Hussein, J. Lubian, and A. Romanelli, "Approximations in fusion and breakup reactions induced by radioactive beams," Nuclear Physics A, vol. 703, no. 3-4, pp. 633-648, 2002.

[76] M. S. Hussein, "Theory of the heavy-ion fusion cross section," Physical Review C, vol. 30, no. 6, pp. 1962-1969, 1984.

[77] G. R. Satchler, "Absorption cross sections and the use of complex potentials in coupled-channels models," Physical Review C, vol.32, no. 6, pp. 2203-2208, 1985.

[78] N. Rowley, G. R. Satchler, and P. H. Stelson, "On the 'distribution of barriers' interpretation of heavy-ion fusion," Physics Letters B, vol. 254, no. 1-2, pp. 25-29, 1991.

[79] H. Timmers, D. Ackermann, S. Beghini, L. Corradi, J. H. He, G. Montagnoli, F. Scarlassara, A. M. Stefanini, and N. Rowley, "A case study of collectivity, transfer and fusion enhancement," Nuclear Physics A, vol. 633, no. 3, pp. 421-445, 1998.

[80] M. Dasgupta, D. J. Hinde, N. Rowley, and A. M. Stefanini, "Measuring barriers to fusion," Annual Review of Nuclear and Particle Science, vol. 48, pp. 401-461, 1998.

[81] R.G. Stokstad, Y. Eisen, S. Kaplanis, D. Pelte, U. Smilansky, and I. Tserruya, "Observation of complete fusion and quasielastic scattering for 200-MeV alpha particles on 208Pb," Physical Review Letters, vol. 41, no. 7, pp. 465-468, 1978.

[82] C.H. Dasso, S. Landowne, and A. Winther, "Theoretical aspects of heavy-ion fusion reactions," Nuclear Physics A, vol. 432, no. 3, pp. 495-526, 1985.

[83] S.G. Steadman, Ed., Fusion Reactions Below the Coulomb Barrier, Berlin: Springer-Verlag, 1984.

[84] M. Beckerman, "Fusion reactions with weakly bound nuclei," Reports on Progress in Physics, vol. 51, no. 3, pp. 281-340, 1993.

[85] P.R.S. Gomes, J. Lubian, L.F. Canto, D.R. Otomar Jr., P.N. de Faria, R. Linares, L. Sigaud, J. Rangel, J.L. Ferreira, and E. Ferioli, "Reactions with weakly bound nuclei, at near barrier energies, and the breakup and transfer influences on the fusion and elastic scattering," Few-Body Systems, vol. 57, no. 3, pp. 165-176, 2016.

[86] S. Kalkal, S. Mandal, N. Madhavan, E. Prasad, S. Verma, A. Jhingan, R. Sandal, S. Nath, J. Gehlot, B.R. Behera, and M. Saxena, "Channel

coupling effects on the fusion excitation functions for Si28+Zr90,94 in sub- and near-barrier regions," Physical Review C, vol. 81, no. 4, p. 044610, 2010.

[87] J.O. Newton, C.R. Morton, M. Dasgupta, J.R. Leigh, J.C. Mein, D.J. Hinde, H. Timmers, and K. Hagino, "Experimental barrier distributions for the fusion of 12C, 16O, 28Si, and 35Cl with 92Zr and coupled-channels analyses," Physical Review C, vol. 64, no. 6, p. 064608, 2001.

[88] J.E. Johnstone, "The influence of shell structure on near-barrier fusion of neutron-rich nuclei" (PhD thesis), Department of Physics, Indiana University, 2022.

[89] S. Mandal, S. Nath, N. Madhavan, J. Gehlot, A. Jhingan, N. Kumar, T. Banerjee, G. Kaur, K.R. Devi, A. Banerjee, and T. Varughese, "Relationship between and effect of inelastic excitations and transfer channels on sub-barrier fusion enhancement," Physical Review C, vol. 96, no. 1, p. 014614, 2017.

[90] H.Q. Zhang, C.J. Lin, F. Yang, H.M. Jia, X.X. Xu, Z.D. Wu, F. Jia, S.T. Zhang, Z.H. Liu, A. Richard, and C. Beck, "Near-barrier fusion of S32+Zr90,96: The effect of multi-neutron transfers in sub-barrier fusion reactions," Physical Review C, vol. 82, no. 5, p. 054609, 2010.

Appendix

A.1 Three Point Difference Method (TPDM) Layout

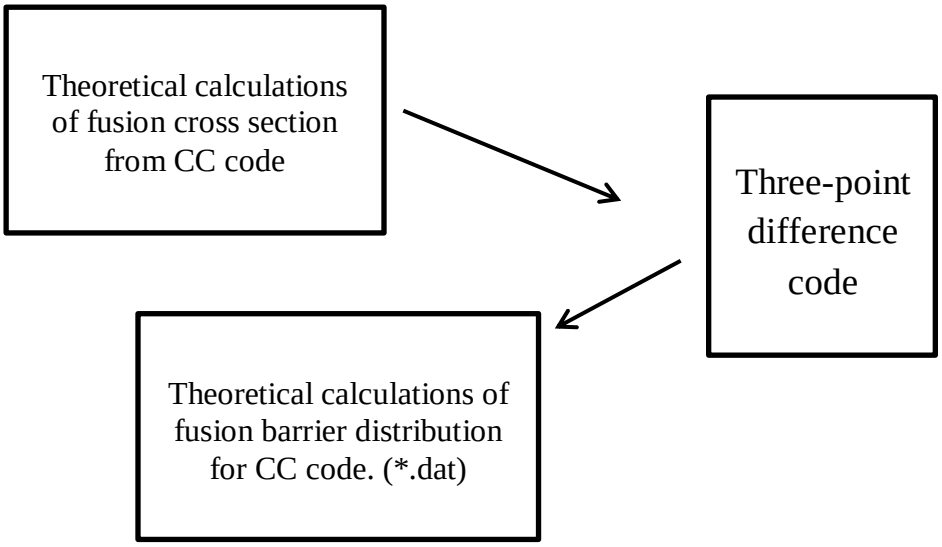

A.2 Three Point Difference Method (TPDM) Flowchart

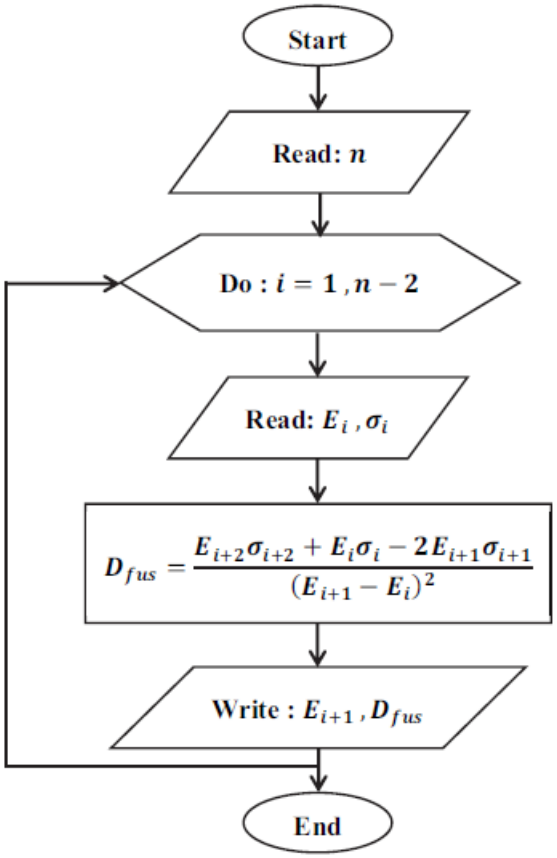

خلاصة

في العمل الحالي ، تم إجراء الحســـابات للمقطع العرضي والانصهار الكلي σ_{fus} وتوزيع حاجز الانصــهار D_{fus} واحتمال الاندماج P_{fus} باســتخدام كل من النهج شــبه الكلاســـــــيكي والميكانيكي الكمومي للأنظمة $^{28}Si+^{90}Zr$, $^{32}S+^{90}Zr$, $^{28}Si+^{96}Zr$, $^{28}Si+^{94}Zr$, $^{28}Si+^{92}Zr$, $^{41}K+^{16}O$, $^{44}Ar+^{28}Si$, $^{45}K+^{28}Si$, $^{41}K+^{28}Si$, $^{35}Cl+^{92}Zr$, $^{32}S+^{96}Zr$ التي تتضـــمن تفاعلات نقل نيوترون واحد أو بروتون واحد.

تـــــضمنت المقـــاربتان شبه الكلاسيكية والميكانيكية الكمية استخدام تقريب Brillouin و Kramers و Wenzel (WKB) لوصف الحركة النسبية بين نواة المقذوف والهدف ، وطريقة القناة المزدوجة المنفصلة (CDCC) من Alder-Winther (AW) لوصف الحركة الجوهرية للنواة. بالنسبة للنهج شبه الكلاسيكي ، تم إجراء الحســـابات باستخدام برنامج الكمبيوتر SCF ، بينما تم إجراء الحسابات الخاصة بالنهج الميكانيكي الكمومي باســتخدام برنامج الكمبيوتر CC ، وكلا البرنامجين مكتوبان بلغة البرمجة (Fortran 90).

تـم تعيين نفس معلمات Wood Saxon لإمكانيات Akyüz Winter لكلا النهجين ، وتمت مقارنة نتائج كلا النهجين مع البيانات التجريبية المقاســة ، عند إضـــافة تأثير الاقتران بين القناة المرنة وقناة التفكك.

وصفت حسابات النهج شبه الكلاسيكي جيدًا جميع الأنظمة المقاسة فوق حاجز كولوم وقد تم تحسين النتائج الموجودة أسفل حاجز كولوم وحوله عندما تم الأخذ بالنظر أقتران القنوات ، بينما بالنســـبة للنهج الميكانيكي الكمومي ، تعزز أداة الاقتران الحســـابات فوق كولوم الحاجز وتحت حاجز كولوم بعيدًا جدًا ولا يمكن وصف البيانات في معظم الأنظمة المدروسة.

جمهورية العراق
وزارة التعليم العالي والبحث العلمي
جامعة بابل
كلية التربية للعلوم الصرفة
قسم الفيزياء

تأثير البروتون والنيوترون كمجس لتفاعلات الاندماج النووي في طاقات قريبة من الحاجز

رسالة مقدمة
الى مجلس كلية التربية للعلوم الصرفة في جامعة بابل
وهي جزء من متطلبات نيل درجة الماجستير
في التربية / الفيزياء

من قبل الطالب

منتظر احمد خضر حسن

بكالوريوس فيزياء/جامعة بابل ٢٠٢٠م

بأشراف

أ.د.فؤاد عطية مجيد

١٤٤٥هـ **٢٠٢٣م**